The Structural Design of Tall and Special Buildings, (2021), e. 1892
https://onlinelibrary.wiley.com/doi/abs/10.1002/tal.1892

Optimal Application of Fluid Viscous Dampers in Tall Buildings Incorporating Integrated Damping Systems

M. Martinez-Paneda[1,2] and A. Y. Elghazouli[2]
[1]*Foster + Partners, Structural Engineering Group*
[2]*Department of Civil and Environmental Engineering, Imperial College London*

Abstract

This paper examines the detailed performance of an Integrated-Damping-System (IDS) approach which was recently introduced to provide large damping levels by enabling two parts of a building to move independently through a parallel arrangement of springs and fluid viscous dampers. Extensive assessments into the characteristics and distribution of constituent dampers are illustrated through the dynamic response of a typical 300m central-core building. Besides examining the system performance under typical wind conditions and selected seismic excitations, five damper placement methods are assessed for various linear and nonlinear damper exponents. It is shown that intermediate exponents provide the best overall response. However, when the design targets a particular damping, deformation or acceleration related performance parameter, specific combinations of damper exponent and distribution can result in an optimal application. Most importantly, due to the underlying IDS nature, which acts as an inherent large-mass damper, the findings show that the overall performance is not highly sensitive to the damper placement and does not necessitate the use of an advanced distribution. Whilst specific placements can be adopted to refine targeted performance aspects where necessary, simple and practical uniform or stiffness proportional arrangements can be consistently employed with the IDS to provide a highly effective solution.

Keywords: tall buildings; multi-storey structures; dynamic response; damping systems; passive damping; mass dampers, fluid viscous dampers; damper arrangement.

1. Introduction

The dynamic response of medium and high-rise buildings under earthquake ground motions and wind-induced excitations can often govern their structural design. Beyond the use of conventional design approaches, such as capacity design to control seismic behaviour or the increase in stiffness to limit wind-induced effects, the deployment of supplementary damping systems can offer an efficient, resilient, and low-damage design solution.

Supplementary damping systems have been applied in many tall buildings worldwide. Since the use of the first elastomeric dampers in the World Trade Centre in 1969, research has focused on the use of viscoelastic dampers to resist seismic and wind-induced vibrations [1]. Since viscoelastic dampers dissipate energy by heat and have highly temperature-dependent properties [2], their use reduced considerably once fluid viscous dampers (FVD) were introduced. One of the first applications of FVDs was in the Torre Mayor building in Mexico, completed in 2003, where they were used as bracing elements up to 20m long [3]. To increase their energy dissipation capacity, other applications included the use of motion amplification devices such as the toggle-brace system, used in the 111 Huntington Avenue building in Boston [4, 5]. Alternative systems also include different applications of viscoelastic dampers or fluid viscous dampers, such as viscoelastic coupling beams [6] using the former, or damped outrigger systems [7] using the latter.

Another common damping system adopted in tall buildings is the Tuned Mass Damper (TMD). This is due to its relatively good performance, simplicity, and adaptability to be added late in the design stage. The first form of vibration absorber which gave origin to TMD was developed by Frahm in 1909 [8, 9]. Since the first TMD was implemented in the John Hancock Tower in 1976 [10], significant additional related research has followed, and different types of TMDs have been developed and employed [11,12]. Examples of these include Multiple TMDs (MTMD) [13], particle TMDs [14], the mega sub-control system [15], or, moving beyond passive approaches, more advanced systems such as active, semi-active or hybrid TMDs [16].

More recently, another approach referred to as the 'Integrated Damping System (IDS)', was introduced by the authors [17], with the aim of combining the merits of FVDs and large-mass TMDs as well as overcoming key limitations of other techniques. The IDS employs part of the existing mass of the building as a damper mass and, by connecting it with springs in parallel with FVDs, generates damping by controlling the differential movements that take place between the damper mass and the rest of the building. The use of springs in parallel with FVDs enables the system to resist the static wind load yet control wind-induced accelerations. Also, rather than providing an additional mass, mobilising a usable part of the building as a damper mass greatly increases the ratio between the damper mass and the building mass beyond that of any conventional TMD. As a result, the IDS system is capable of providing considerable levels of additional damping with minimal differential displacements. At the same time, unlike conventional TMDs, the IDS system does not add mass to the building and is therefore fully integrated within the design without occupying any valuable space.

Another key advantage of the IDS is that, due to its inherent large mass ratio, the performance is less dependent on the optimum frequency tuning of the damper mass compared to conventional TMDs [17]. Accordingly, the spring stiffness can be set primarily to control the maximum level of differential displacement whilst still providing significant supplementary damping levels. In contrast to other systems, such as continuously damped arrangements which rely on overall flexible buildings, or outrigger engagement systems which are restricted by the resistance to static loads, the IDS system does not rely on a reduced overall building stiffness and is hence applicable to both tall and supertall buildings. Moreover, unlike conventional TMDs, the IDS is largely insensitive to detuning and provides a robust response irrespective of changes in the dynamic characteristics of the structure, while being able to effectively control both wind and seismic excitations.

Within the IDS, the stiffness of the spring elements is largely fixed as these are set to control displacement under static wind loads. FVDs, on the other hand, do not have any pre-imposed requirement besides that of controlling accelerations within the damper mass. Optimal design, placement, and sizing of FVDs have been extensively investigated in recent years. A significant part of this effort has focused on the damper coefficient (c) considered as a measure of damper cost and directly related to the level of additional damping. Damper placement strategies and tuning of their mechanical properties have also proven to have a significant impact on both the structural behaviour and the total damper cost [18]. The largest body of research has focused on placement in low or mid-rise buildings undergoing shear-type deformations, typically the most common for FVD applications. Some researchers have also extended this to buildings with flexural-type deformations [19, 20]. From the early studies in the 1980s and 1990s, most of the research has focused on planar linear buildings with linear dampers [21, 22]. Research was subsequently expanded to consider nonlinear damper properties [e.g. 23, 24], nonlinear structural behaviour [e.g. 25, 26] or irregular three-dimensional structures [e.g. 27-29].

Many studies have compared the performance of the various placement methods, with different outcomes depending on the target performance index [e.g. 30-32]. Following the categorization suggested by Domenico et al. [33], height-wise damper distribution design methodologies can be grouped into 'heuristic', 'analytical', and 'evolutionary'. Heuristic approaches exploit some problem-specific knowledge of the structural behaviour, and are generally characterized by practicality and simplicity, hence they can be used with minimum computational effort. They include the uniform damper distribution or the story-shear-strain-energy [34]. With a more refined formulation, analytical approaches include the method developed by Gluck et al. [35], which adopts optimal control theory, the gradient-based search procedure proposed by Takewaki [36], and the fully-stressed analysis-redesign technique suggested by Levy & Lavan [37]. On the other hand, evolutionary methods are primarily genetic algorithms based on natural biological evolution and operate on a population of potential solutions without computing any gradient. Although they tend to provide better results, these methods require a notably increased computational effort [38-40].

In addition to the damper coefficient, the damper exponent (α) can also play a major role in the FVD performance. Linear dampers are generally more capable of suppressing higher modes and have the benefit of being offset with peak structural forces that are concurrent with maximum displacements [41]. However, linear dampers have the disadvantage of developing large forces under moderate or severe earthquakes, forces which can exceed the building or damper capacity, hence jeopardizing the system and its energy-dissipation capabilities, particularly for long period structures [42]. Two different methods can be implemented to reduce the damper forces, either to use a nonlinear viscous damper or to limit the maximum output force by means of a release or control valve. While some applications such as the Philippines' St Francis Plaza towers [7] have included release valves, nonlinear dampers tend to become a more cost-effective option. The damper exponent typically varies between 0.1 and 2, and is usually achieved either by modifying the damper material or by adapting the damper structure [21].

Initial studies by Symans & Constantinou [44] have shown that nonlinear viscous dampers outperform linear counterparts in terms of damper forces and supplementary damping. Typical damper exponents for seismic applications are within the range of 0.35 to 0.7 for shear buildings. However, it should be noted that, while for a conventional structure the forces decrease with a lower damper exponent, the inter-storey drifts, and hence the level of damage and building instability increases. Accordingly, significantly low damper exponents are not recommended, and the taller the building the higher is the suggested exponent value [45].

Although the fundamental principles and underlying formulations of the IDS system have been introduced in a previous study [17], its application in practice necessitates a detailed assessment of the influence of damper characteristics and arrangement on the dynamic response. While optimal damper procedures have been widely evaluated for conventional buildings [33], such investigations for the proposed IDS system or, more broadly, for large-mass TMDs are currently lacking. This paper therefore examines the performance of the IDS approach, with a particular focus on the constituent FVDs characteristics. In order to provide a practical perspective and detailed insights into the behaviour, the assessments are illustrated through the dynamic response of a typical 300m tall building incorporating the IDS alongside a conventional internal core arrangement. The key parameters related to the FVDs performance, as well as their alternative placement methods within a structure, are first discussed. This is followed by detailed assessments with respect to the optimal damper parameters and arrangement. Based on the findings, the main recommendations and implications for practical application are highlighted.

2. Fluid Viscous Dampers

Fluid viscous dampers (FVD) are passive energy dissipation systems that have long been used in military applications and are now well established in civil engineering [46-48]. Fluid viscous dampers are relatively well-known devices, and details on their hydrodynamics, energy dissipation mechanisms, and design developments can be readily found in the literature [43]. Some of the merits behind their common use are their large energy dissipation capacity with small movements, the offset between the maximum damper forces and structural forces, and their lack of static stiffness with excitation below a cut-off frequency of 4 Hz [44] hence not altering the building stiffness characteristics. FVDs, and supplementary damping systems more generally, offer improved structural performance whilst providing a low or no damage solution, hence resulting in efficient life-cycle costs when considering post-earthquake repair and business interruption implications [49].

Fluid Viscous Dampers can be categorised as linear or nonlinear depending on the value of the damper exponent, α. The damper output force is defined by the following widely recognised relationship (Eq. 1):

$$F_d = c \cdot sign(V) \cdot |V|^{\alpha} \quad (1)$$

Where F_d represents the damper force, c is the damper coefficient, sign() is the velocity sign, V is the differential velocity between both ends of the damper, and α is the damper exponent. The force-velocity relationship normalised over the damper coefficient is depicted in Figure 1 for representative damper exponent values of 0.2, 0.5, 1, and 2.

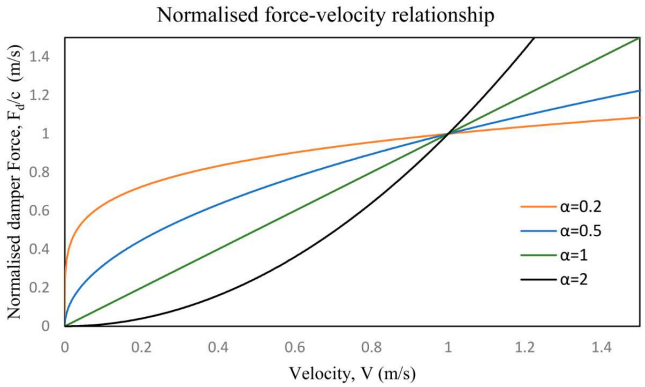

Figure 1: Damper force, normalised by the damper coefficient, versus velocity

To further illustrate the FVD behaviour, it is also useful to plot the energy dissipated under a harmonic motion for the different damper exponents as depicted in Figure 2. This is estimated using Equation (2) where u and V represent the displacement and the velocity as a function of time, respectively; u_0 is the amplitude, w the natural circular frequency, and t the time. From the hysteresis loops in Figure 2a, it is shown that fluid viscous dampers with a lower damper exponent absorb more energy per cycle than one with a higher exponent for a constant damper coefficient. However, it is important to note that, while the latter is true for small displacements, as the movement amplitude increases, the velocity increases. Relating this to Equation (1), and as shown in Figure 2b, it is evident that for large movement amplitudes an exponent larger than 1 can result in increased energy dissipation. While this can lead to higher forces, the use of a lower damper exponent would result in a negligible level of damping as recognised in previous studies [6].

$$u(t) = u_0 \cdot \sin(wt) \qquad V(t) = wu_0 \cdot \cos(wt) \tag{2}$$

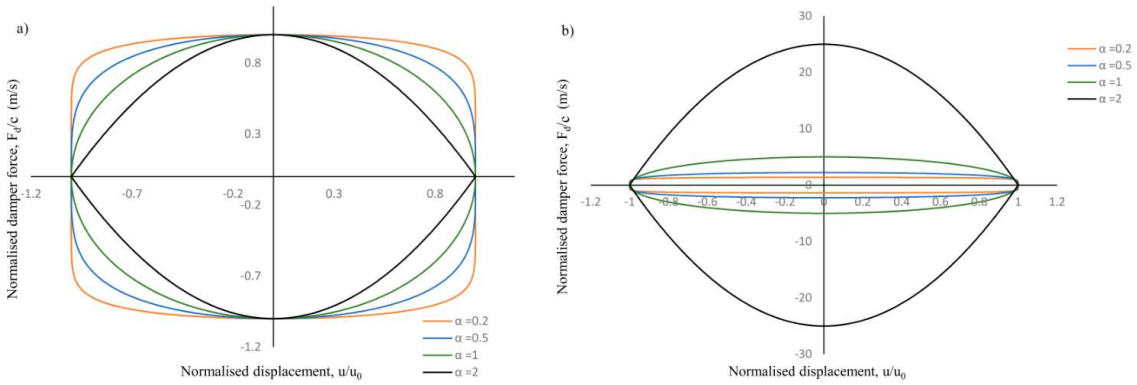

Figure 2: Hysteresis loops for fluid viscous dampers for different damper exponent values under harmonic motion and constant frequency: a) For amplitude $u_0 = 1$, b) for amplitude $u_0 = 5$.

2.1 Damper coefficient and placement method

As noted in the introduction, various placement methods have been proposed for the distribution of FVDs in building structures. However, the present study only focuses on heuristic and analytical approaches given their relative recognition and accessibility for practicing engineers, although it is recognised that the adoption of more advanced and refined methods could be of benefit. Five placement methods are selected and discussed below based on their suitability, accuracy, and efficiency.

(i) *Uniform distribution (UD):* This is the simplest placement technique, in which the FVDs are identical at every storey. While this method may not be as effective as others in terms of total damper cost, it is one of the most commonly used and often serves as a benchmark. The damper coefficient at each storey, c_j, is directly calculated from the total damper coefficient value, c_t, divided by the number of storeys, n_s (Equation 3).

$$c_j = \frac{c_t}{n_s} \tag{3}$$

(ii) Stiffness proportional distribution (SPD): In this case, the damper coefficient values are assigned in proportion to the relative storey stiffness. The damper coefficient at each floor is equal to the ratio between the stiffness of that floor, k_i, and the sum of the stiffnesses of all the damped floors, multiplied by the total added damping (Equation 4).

$$c_j = \frac{k_j}{\sum_i k_i} c_t \tag{4}$$

(iii) Storey shear strain-energy method (SSSE): The SSSE distribution allocates the damper coefficient along the building height in proportion to the storey shear strain energy corresponding to the first mode of vibration of the structure. By using Equation 5, it is possible to calculate the storey damper coefficient, c_j, where φ_{rj} is the relative modal displacement of Storey j, and S_j is a storey parameter proportional to the shear force $=\sum_{i=j}^{roof} m_i \varphi_i$, where m_i is the mass of the i^{th} storey and φ_i is the modal displacement.

$$c_j = \frac{S_j \varphi_{rj}}{\sum_i S_i \varphi_{ri}} c_t \tag{5}$$

(iv) Simplified Sequential Search Algorithm (SSSA): Based on the Sequential Search Algorithm [50], and since linear viscous dampers are essentially velocity-dependent devices, their energy dissipation capabilities would be maximised at locations where inter-storey velocities are largest [51, 52]. The damper location is hence defined by a sequential procedure where the seismic response of the structure is evaluated such that damper increments of the same size are placed sequentially at the points of maximum inter-storey velocity until all dampers have been allocated.

(v) Fully-stressed analysis-redesign algorithm (FSDA): This method uses an iterative procedure to maximize, i.e. "fully stress", the effect of the dampers by using a recurrence relationship based on a performance index parameter (e.g., inter-storey drift or acceleration response) [37]. The damper coefficient value for the next iteration at a storey i, $c_i^{(n+1)}$, is defined by Equation 6, where n represents the iteration number, $pi_i^{(n)}$ is the actual i^{th} component of the performance index at the n^{th} iteration, and q is a convergence factor that can be typically selected as 0.5 for linear problems and 5 for nonlinear cases [37].

$$c_j^{n+1} = c_j^n \ \left(\mathrm{pi}_\mathrm{j}^\mathrm{n}\right)^{\frac{1}{\mathrm{q}}} \tag{6}$$

It should be noted that the above techniques are conceived for the placement of linear dampers and represent those that are most widely used in practice. Although with some slight modifications they can be optimally adjusted to offer better results for nonlinear damper allocation, for simplicity, the current formulations are retained herein, particularly since the results are not expected to differ notably as shown in previous studies [33, 40].

Conventional methods aim to place FVDs at locations with large differential motions and without additional elements that could act as alternative load paths. This is because having a spring in parallel with the FVD forming a spring fluid viscous damper significantly reduces the level of damping [6]. However, it is important to note that this is not detrimental for structures incorporating the IDS approach considered herein. This is because by having a spring in parallel, the system is able to mobilise a far larger damper mass. Hence, although a small portion of the maximum damping that could be achieved is obtained, this is still typically sufficient to control the dynamic response of tall buildings. While previous studies have assessed various damper optimisation methods, such investigations are lacking with respect to spring fluid viscous dampers. There is also a need to examine the application of damper placement methods in large mass damping systems and, more specifically, to the IDS approach dealt with in this study.

3. Integrated Damping System

The underlying principle of the Integrated Damping System (IDS) is to have an identifiable movable mass, which is part of the inherent own mass of the building and could move differentially from the lateral force-resisting system. The IDS approach, introduced recently by the authors [17], was, for simplicity, originally illustrated using a building with a mega-frame as lateral force resisting system, which was external to the office floors. In addition to assessing optimal damper characteristics and placement arrangements, this study also introduces and examines the application of IDS to a typical central-core configuration, which is one of the most common typologies used for tall buildings. For such structures, the core is the main resisting element and, unless also engaged by outriggers

to the core, the perimeter columns are typically considered as secondary elements that do not contribute notably to the lateral force-resisting system.

For the purpose of the assessments undertaken herein, an illustrative 300m tall building with a central core is considered, as depicted in Figure 3. The building footprint is 54m x 54m, with the core located at the centre of the floor plan, with dimensions of 20m x 20m. This results in a height-to-core depth ratio of 15. Typical central core buildings have reinforced concrete cores, partly to supply the required lateral stiffness and resistance whilst also providing mass to control wind-induced accelerations. However, if accelerations are no longer a critical issue due to the implementation of a supplementary damping system, a more efficient tall building can be designed with a steel core. Besides savings in foundations due to a lighter tower, other benefits include the relatively faster construction speed associated with steel towers. Apart from the merits in terms of saving in foundations, due to the lighter weight, as well as the faster construction speed, other benefits of all-steel towers are being increasingly recognised, including the lower construction waste and improved recyclability and re-use that can result in a lower carbon footprint once the overall lifecycle of the structure is considered.

As shown in Figure 3, the building considered has a steel braced core and consists of 65 floors with a typical floor-to-floor height of 4.5m. At the ground floor, and the transition between Tiers 2 and 3, there are 9m tall double-height floors. The building was preliminary designed using the widely-used commercial design software ETABS [56] according to EN 1993-1-1 provisions [57]. The floors were designed as composite steel/concrete, with lightweight concrete topping in the lower tiers and normal-weight concrete in the third tier. The office floors were designed as single-span with secondary beams sized as HEA 700, edge beams as HEB 700, and primary beams as HEM 700 [58]. The perimeter and core columns were designed as concrete-filled steel tube (CFT) sections to match the construction process, yet still benefit from the concrete compression capacity. The exterior columns taper with the height, as strictly required to resist the gravity loads. The interior core columns and braces were sized to satisfy a top displacement limit of H/500 under wind loading, and a maximum height/300 inter-storey drift using the 50-year London wind base speed of 21.4 m/s, as defined in the UK NA to EN 19901-1-4 [59].

The details of the building in terms of heights, tiers, core column, brace and beam sizes, and core and floor masses are defined in Table 1. The mechanical properties of the materials employed are included in Table 2. The modal participation mass ratios and the natural periods for the first six modes of vibration are given in Table 3. As indicated in Table 2, the building has a relatively long fundamental period of nearly 10 seconds as a result of the flexibility of the slender steel core. The first two modes are translational, in the diagonal direction, and well separated from the third torsional mode without any torsional coupling. Such a tall building would not typically be feasible in practice as it would most likely experience excessive wind-induced accelerations. To this end, these accelerations were checked following the NBCC 2010 provisions [60] with an assumed intrinsic damping of 0.8% representative of a steel building of this height [61]. The estimated across-wind acceleration for a one-year return period was determined as 17.7 mg, which is well above both the 1-year conventional practice limits [62] and the ISO 10137:2007 recommendations [63]. For such a situation, the implementation of a damping system is identified as an ideal solution to control wind-induced vibrations to an acceptable level and hence permit the use of such a light and efficient design.

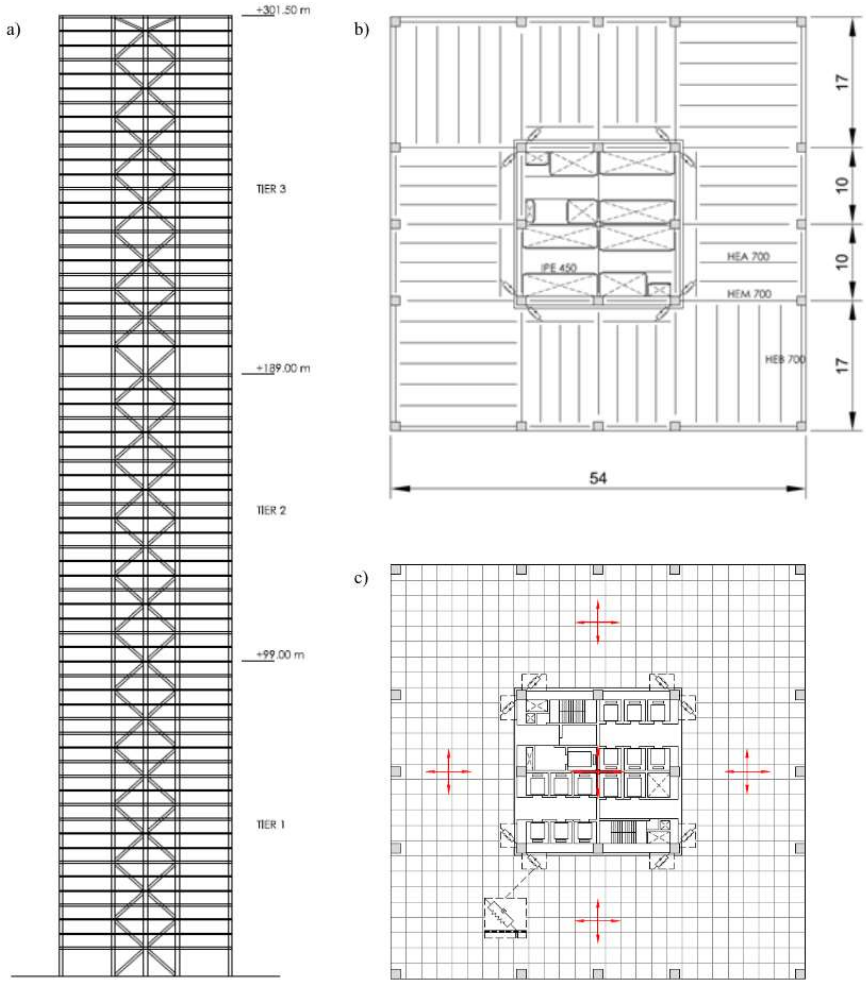

Figure 3: Investigated tall building geometry. a) Elevation, b) Typical structural floor plan, c) IDS implementation. (dimensions in metres)

Table 1: Details of selected building

Storeys, i	Elevation [m]	Tier	Core column	Core Brace	Core Beam	Core mass, $m_{c,i}$ [kg]	Floor mass, $m_{f,i}$ [kg]
65	301.5	3	CFT 1000x50	H 700x700x60x60	H 500x250x10x18	153664	1653354
64	297	3	CFT 1000x50	H 700x700x60x60	H 500x250x10x18	165904	1672682
54 to 63	252 to 292.5	3	CFT 1000x50	H 700x700x60x60	H 500x250x10x18	170544	1672682
53	247.5	3	CFT 1200x70	H 700x700x60x60	H 500x250x10x18	188170	1672682
43 to 52	202.5 to 243	3	CFT 1200x70	H 700x700x60x60	H 500x250x10x18	206029	1679717
42	198	3	CFT 1200x70	H 700x700x60x60	H 500x250x10x18	340387	1723794
41	189	2	CFT 1600x80	H 800x800x80x80	H 500x250x10x18	301006	1586227
33 to 40	153 to 184.5	2	CFT 1600x80	H 800x800x80x80	H 500x250x10x18	279114	1563316
32	148.5	2	CFT 1900x100	H 800x800x80x80	H 500x250x10x18	311771	1572238
22 to 31	103.5	2	CFT 1900x100	H 800x800x80x80	H 500x250x10x18	344775	1584789
21	99	1	CFT 2000x125	H 1000x1000x80x80	H 500x250x10x18	410805	1599160
12 to 20	58.5 to 94.5	1	CFT 2000x125	H 1000x1000x80x80	H 500x250x10x18	476982	1605326
11	54	1	CFT 2000x140	H 1000x1000x80x80	H 500x250x10x18	467319	1618420
2 to 10	13.5 to 49.5	1	CFT 2000x140	H 1000x1000x80x80	H 500x250x10x18	457655	1636496
1	9	1	CFT 2000x140	H 1000x1000x80x80	H 500x250x10x18	702930	1721794

Table 2: Material properties

Elements	Grade	Modulus of Elasticity, E	Density	Concrete strength, f_{ck}	Yield strength, f_y
Lightweight slab on metal deck	C30/37	23 335 MPa	18.5 kN/m^3	30 MPa	-
Normal-weight slab on metal deck	C30/37	33 000 MPa	23.5 kN/m^3	30 MPa	-
CFT columns concrete infill	C80/95	42 000 MPa	25.0 kN/m^3	80 MPa	-
Steel rolled and plate sections	S355	210 000 MPa	76.9 kN/m^3	-	355 MPa

Table 3: Modal participation mass ratios

Mode	Period [s]	UX	UY	RZ
1	9.9	36 %	23 %	0 %
2	9.9	23 %	36 %	0 %
3	5.0	0 %	0 %	77 %
4	2.4	0 %	21 %	0 %
5	2.4	21 %	0 %	0 %
6	1.9	0 %	0 %	12 %

As noted previously, this typical illustrative tall building was selected in order to further assess the performance of the Integrated Damping System (IDS) by implementing it between the office floors and the core. With all the perimeter columns designed and idealised as pin-ended, the lateral stability of the office floors is provided solely by the central core. As shown in Figure 3c, a gap is placed between the core and the office floor to avoid pounding. The office floors and the core are also connected by a series of FVDs in parallel with springs disposed at 45 degrees. This 45-degree arrangement increases the damper end displacements in order to maximise the energy dissipation capacity and also enables the IDS to provide damping in the torsional vibration mode, which many conventional systems fail to mitigate. Although the IDS could be applied throughout the whole height, this is only implemented herein in the top (i.e. third) tier for simplicity of the design. It is also worth noting that although the present study has adopted a regular building and damper configuration that can be easily extrapolated to most building types, this might not be the case for highly irregular buildings or those that could exhibit a significantly different dynamic behaviour.

4. Modelling Procedures

The dynamic response of the tall building, incorporating the IDS system, with a focus on the influence of the FVD damper characteristics and arrangement, is examined herein using the idealised numerical model depicted in Figure 4. The building core and floors are separately modelled as lumped masses at their respective heights and connected with either rigid links (at the first two tiers) or using a damper in parallel with a spring (for the third tier). The mass of the core is denoted as $m_{c,i}$, the mass of the office floors as $m_{f,i}$, the damper coefficient as c_i, the spring in parallel with the damper as $k_{f,i}$, the rigid links as k_R, and the core stiffness as $k_{c,i}$, where i represents the storey number. Although the response of tall or supertall buildings cannot be fully characterised using a planar model, as it cannot capture the torsional or coupling effects, this is considered herein for simplicity, particularly given the focus on the comparative influence of key parameters that can be fully captured by the adopted model. The ability of the system to generate damping in the torsional mode is identified as another major benefit which is yet to be investigated, as it is beyond the scope of this study and would require the use of detailed 3D models. The idealised structure is modelled using the commercial finite element software SAP2000 [64]. Since this software is widely used in practice, the model and the results can also be replicated and examined for different configurations by design engineers. To ensure the reliability of the simplified model, it was benchmarked against the detailed 3D model of the structure. The total mass and mass distributions were exactly matched in both models. As indicated in Table 4, the translational modal periods in the two models were within acceptable margins for tall building design.

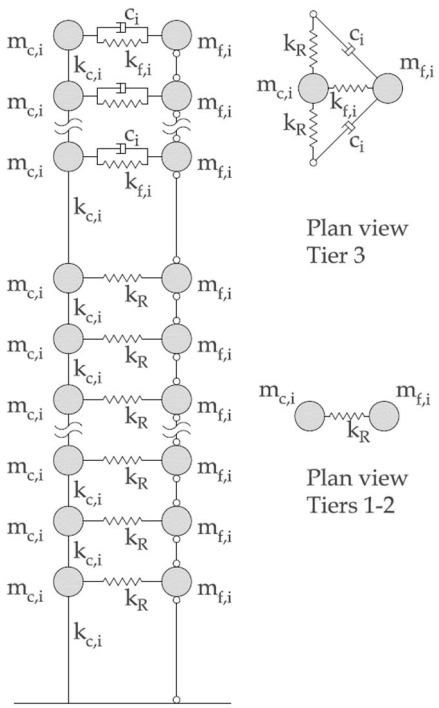

Figure 4: Idealised model representation of the tall building for dynamic analysis

Table 4: Translational modal periods comparison

3D model		Simplified model		
Mode	Period [s]	Mode	Period [s]	Difference
1	9.9	1	10.3	4 %
4	2.4	2	2.5	4 %
8	1.1	3	1.2	7 %

To determine the level of additional damping that the system is able to generate, the model was first subjected to a series of time history sweep excitations. This was performed for each considered damper coefficient and exponent values for a range around the fundamental natural frequency of the structure under a first mode deformed shape load pattern. This load pattern was applied with an amplitude which followed a sine excitation through the time history and a period which matched the inverse of the excitation frequency. The analysis continued until a steady-state response for that specific frequency was reached. The half-power bandwidth method was then used to calculate the overall damping from the sweep curve obtained from the steady-state peak response of each excitation frequency [65].

The optimal damper coefficient to maximise additional equivalent damping was then used to assess the building response under seven real earthquake acceleration time histories. The records were selected to match closely the EN1998-1 Type 1 Soil C target spectrum [66], minimizing the normalised root mean square deviation, D_{RMS}, over a period range from 2 to 10 s [67], with a magnitude, M, from 5.0 to 7.5; a distance from the fault from 10 to 100 km, and a shear wave velocity, Vs, from 180 to 800 m/s. All response spectra were scaled to match closely the EC8 response spectrum with a peak ground acceleration of 0.25g [68]. It is important to note that such code defined response spectra are not typically intended for use beyond a period of 4 seconds. However, the response spectrum is used herein as a comparative benchmark to scale the seismic records, noting that each damper configuration is compared using the same excitations. As is common practice, seismic demands should be based on a site-specific seismic hazard assessment for actual practical applications on tall buildings with such long periods. The intensity of the event determines the magnitude of movement and hence the level of additional damping; the larger the movement the larger is the additional damping generated. Also, the type of seismic excitation, e.g. cyclic or pulse dominated, can affect the system response. This was accounted for by selecting different types of excitations within the prescribed parameters. The unscaled time-history records and response spectra are shown in Figure 5, while their seismological data, scaling factors, and corresponding D_{RMS} values are provided in Table 5. As mentioned before, the mean spectrum of the seven records matches that of the EC8

spectrum. The variation in record selection can be observed in the table by noticing how records 00127 T and 00302 T result in large scaling factors due to their reduced energy content within the long period range. Although such large scaling factors should typically be avoided if possible, as noted before, these scaled records are used herein for comparative purposes whereby each damper configuration is compared to the same excitations.

Five performance indexes were selected to represent the building performance: top displacement, inter-storey drifts, absolute accelerations, differential displacements, and damper force. The top displacement is selected as a measure of the overall building response and calculated at the core throughout the time history analysis. The inter-storey drift is determined as the ratio of the maximum differential displacement between consecutive floors at every time step over the entire time history, normalised by the storey height. The absolute accelerations and the inter-storey drifts are related to the comfort of occupants as well as the damage to structural and non-structural elements. Floor accelerations are taken as the maximum value of the absolute accelerations over the entire time-history response for each floor. The differential displacement is calculated as the maximum differential movement between the movable office floors and the core throughout the time-history. Damper forces are extracted as the maximum value throughout the excitation for each damper.

Table 5: Seismological and scaling data for the seven selected records

NGA Record No.	Earthquake Name	Date	Magnitude	Distance to Fault (km)	V_{s30} (m/s)	PGA (g)	Scale Factor	D_{RMS}
00127 T	Friuli, Italy	1976-09-11	5.5	15.1	339	0.04	8.72	0.28
00138 L	Tabas, Iran	1978-09-16	7.4	24.1	339	0.11	1.08	0.28
00293 T	Irpinia, Italy	1980-11-23	6.9	59.6	660	0.05	1.14	0.37
00302 T	Irpinia, Italy	1980-11-23	6.2	22.7	339	0.10	7.36	0.27
00564 L	Kalamata, Greece	1986-09-13	6.2	11.2	339	0.25	1.84	0.18
01144 L	Gulf of Aqaba	1995-11-22	7.2	43.3	355	0.10	1.88	0.19
01155L	Kocaeli, Turkey	1999-08-17	7.5	60.5	275	0.10	0.61	0.33

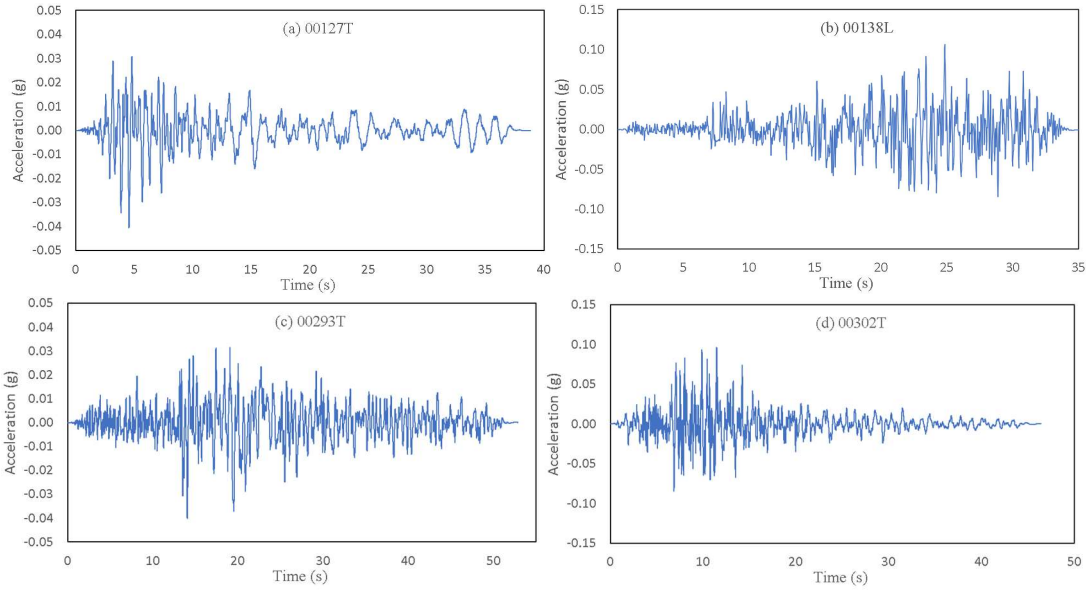

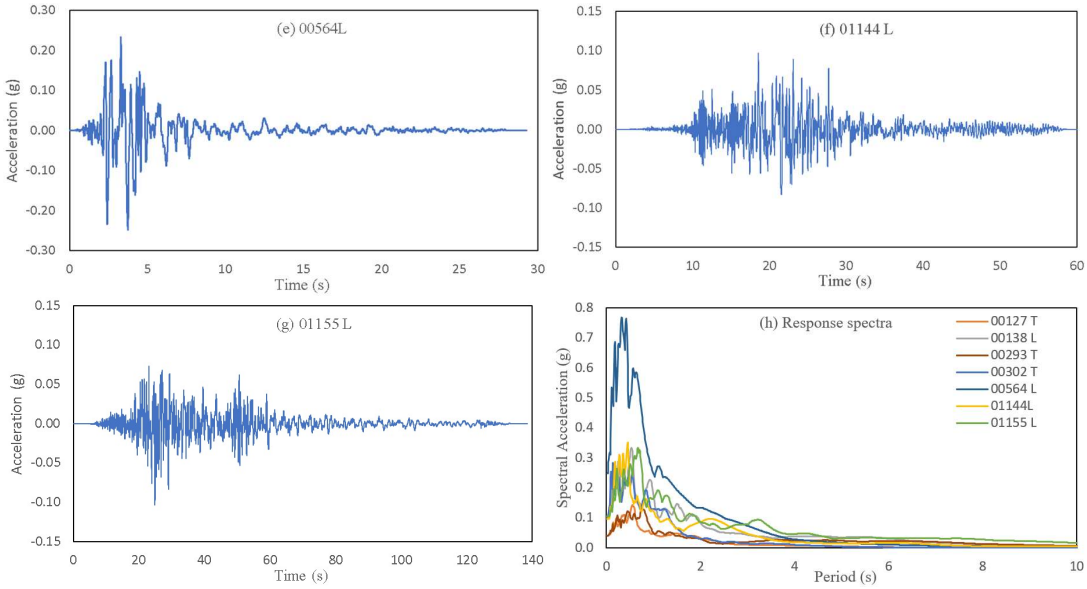

Figure 5: Unscaled acceleration-time histories for the seven selected records (a-g) and corresponding response spectra (h)

4.1 Brace stiffness

Dampers are typically represented using a Maxwell model formed by a linear spring in series with a nonlinear dashpot system to capture the effect of damper and brace stiffness in the formulation [53-55]. The brace stiffness, k_b, and its relationship with the damper coefficient, c, and the parallel spring, k_f, is investigated herein as a function of the equivalent damping, ξ_e, of the building. The equivalent damping is calculated using the half-power bandwidth method with a constant damper coefficient and a varying brace stiffness. The damper coefficients are selected as the optimum to maximise the additional equivalent damping for each damper exponent assuming a uniform damper distribution.

The results are depicted in Figure 6a as a function of the relaxation time constant, which is the ratio between damper coefficient and brace stiffness, $\tau_d = c_i/k_{b,i}$, versus the equivalent damping ratio for each of the damper exponents [53]. The plot shows that a very flexible brace stiffness for FVDs cannot generate any damping. As the brace stiffness increases, their contribution starts to grow to reach a plateau beyond which no difference occurs for harmonic excitations where the brace does not reach the lock-in frequency. The relaxation time constant for linear cases and $\alpha = 0.5$ are observed to be in the same range as those indicated by Singh et al. [54] as common from FVD manufacturers for conventional applications. However, it is worth noting that the optimum τ_d values vary for $\alpha = 0.2$ and $\alpha = 2$. This may be attributed to the fact that the considered optimal damper coefficients vary considerably from one exponent to the other, and that its efficiency is also related to the absolute value as well as its relationship with the parallel spring. The variability of the damper coefficient is removed in Figure 6b, where the equivalent damping is plotted against the relaxation time constant for the four considered damper exponents under a constant damper coefficient value (taken as the optimum for $\alpha = 1$). It is interesting to note that the relaxation time constant value for optimal results is related to the damper exponent, and the lower α is the lower the minimum optimum τ_d will be. Although some research has noted related issues [28, 53, 69, 70], there appear to be considerable gaps on this in the literature.

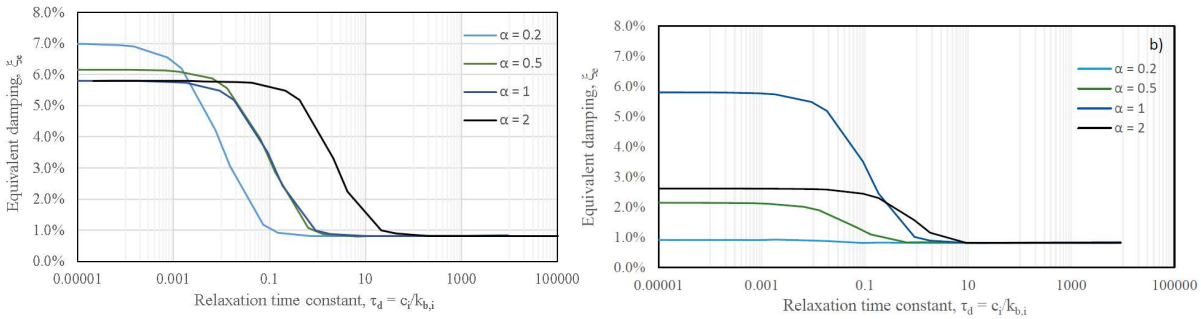

Figure 6: Influence of brace stiffness on equivalent damping, ξ_e, for the IDS system with: a) optimal damper coefficient, b) equal damper coefficient for all damper exponents

Based on the above results, a relaxation time constant of 0.01 is used for all damper exponents except for $\alpha = 0.2$. Because of its significantly reduced damper coefficient, it is possible to provide a larger stiffness value hence a value of $\tau_d = 0.001$ is utilised.

4.2 Damper placement methods

The optimal damper placement can depend on the nature of the excitation, hence an ideal arrangement for a specific excitation may not be optimal for another. To overcome this issue when investigating optimal damper placement, the concept of critical excitation has been considered in previous studies [71]. Some methods, such as the FSDA, allow more than one excitation to be captured within their iterative formulation by evaluating the distribution using a time history analysis and incorporating them into the active set if they exceed the previous demand [37]. While this applies to low-rise buildings, for tall buildings, and especially those subjected to wind excitations as well, the first mode would largely control the response. Taking this into consideration, for the current study, instead of optimising to a single or a set of specific ground motions, a more efficient solution is identified by setting the performance target index as the first mode level of additional supplementary damping. Apart from the first mode damping being the most relevant for the building under wind excitation, the use of such index also provides a measurable target that is independent of the seismic excitation.

Based on the above discussion, damper placement methods are investigated herein under a first mode resonance corresponding to a first mode deformed shape load pattern. This approach differs from conventional damper placement approaches as, although flexural buildings were considered before, these were for much lower-rise structures and focused on the seismic excitation itself rather than also on wind and hence first mode damping. Taking this into consideration, the SSSA method is adapted from conventional applications to account for dampers located within the same level. Differential velocities between both ends of the spring-damper arrangement are also considered rather than inter-storey velocities.

The FSDA formulation is modified from its basic expression (as described in Section 2) to account for the total level of damping and avoid dependency on the allowable inter-storey drift limit if the value is equal for all storeys (Equation 7) [32]. Besides this, and as applicable to the present case, the performance index is shifted from the inter-storey drift to the differential displacement between the core and the movable floors, d_i^k.

$$c_i^{k+1} = c_i^k \left(d_i^k\right)^{\frac{1}{q}} \frac{c_t}{\sum_i c_i^k (d_i^k)^{\frac{1}{q}}} \tag{7}$$

The five different placement methods are tested for a range of total damper coefficient values from which the optimum (in terms of maximising additional damping) is selected and further investigated in subsequent sections. As dampers also perform the function of controlling accelerations, the FSDA and SSSA methods are stipulated to have a minimum damper coefficient per storey of 50 kNs/m, which is identified as a minimum to limit acceleration levels.

5. Parametric Assessments

5.1 Equivalent damping

The stiffness of the spring joining the core and the movable floor mass is one of the key parameters determining the performance of the system. In introducing the IDS approach, the authors [17] initially investigated two cases that represented upper and lower bounds considering implementation feasibility. For the present study, in order to focus on assessing the influence of other key parameters, an intermediate practical value for the spring stiffness was set at each floor such that a maximum movement of 150mm occurs under the 50-year return period wind load according to EN1991-1-4 [59]. Although this value could be exceeded under the Risk-Targeted Maximum Considered Earthquake (MCER), it was selected as a representative value that can ensure occupant comfort and lies within conventional movement joints splices for services. The level of additional equivalent damping is investigated for four damper exponents, α, of 0.2, 0.5, 1, and 2, with the same floor spring yet varying the damper coefficient and distribution. The resulting first mode equivalent damping for each damper exponent and placement method is depicted in Figure 7.

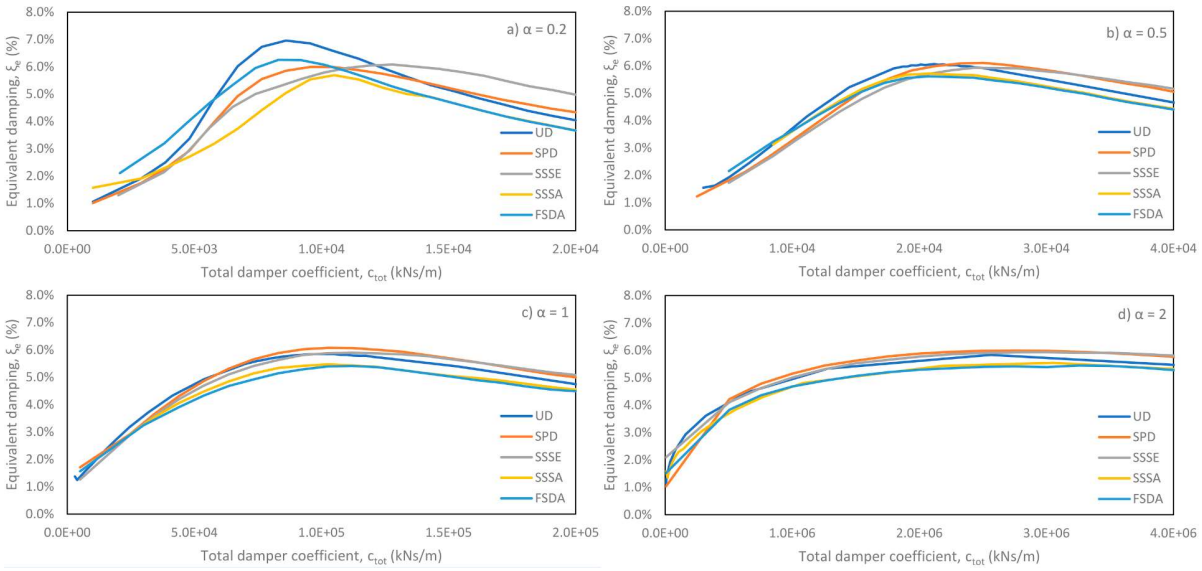

Figure 7:Equivalent damping versus damper coefficient for damper exponent values of a) 0.2, b) 0.5, c) 1 and d)2 using the five damper placement methods

From the results, it can be observed that, for the considered maximum differential displacement, the largest level of equivalent damping, 7%, is obtained with a 0.2 damper exponent and dampers uniformly distributed along the height (UD). From the plots, it is also worth noting that although all damper exponents achieve a broadly similar level of additional damping, the optimal total damper coefficient increases with the increase in damper exponent. Although many studies [38, 72] consider the total damper coefficient as a measure of cost, this is not necessarily the case when accounting for different damper exponents. However, since damper forces are tied to the damper coefficient, as indicated in Equation (1), a lower damper exponent would have the added benefit of resulting in lower damper forces. To this end, for a given damper exponent, it is also worth noting that all placement methods achieve their optimum result at a broadly similar total damper coefficient value.

The results in Figure 7 also indicate that despite the simplicity of the uniform damper distribution method, it still offers very good results, which are only exceeded marginally at higher damper exponents by SSSE and SPD. Although SSSA and FSDA are methods that, for conventional buildings, typically provide better results than more simple approaches such as UD, they are not superior to other techniques in terms of maximising the additional equivalent damping. This is attributed to both methods being intended for maximising energy dissipation by the FVD, e.g. allocating dampers where the inter-storey velocities are larger for the SSSA. However, the FVD is not the only mechanism within the IDS system and, as indicated, the large-mass TMD behaviour plays a major role.

Further insights into the behaviour can be obtained once the optimal damper distributions for each damper exponent and placement method are plotted with respect to the total damper coefficient per storey, as illustrated in Figure 8 a-d as well as in Tables 6 and 7. As depicted in the plots, FSDA and SSSA allocate a larger damper coefficient to the higher floors as drifts and velocities are larger due to the higher amplitude. While this is efficient for maximising energy dissipation, it also limits the TMD behaviour as it constrains the movement of the upper floors. Besides their larger amplitude, this is also of particular importance since the higher floors are the most effective when the mass ratio between the damper mass and fixed mass is normalized by their contribution to the modal mass. As expected, for the same level of motion and mass, the higher the mass is placed the more effective it will be. The SSSE approach follows an inverted approach, compared to FSDA and SSSA, as its larger total damper coefficient is allocated mostly to the lower storeys while the higher storeys are lower than UD. In this case, the lower storeys, with a less effective mass ratio, can accommodate a higher damper coefficient and benefit from it, while the higher storeys benefit from a reduced damper restraint. The SPD method, on the other hand, gives very similar results to the UD approach since it is based on the differential stiffnesses and these, being designed to resist the static wind load, are relatively uniform along the height. However, as the top floor has less tributary height and the connecting spring is designed to meet the same performance target, the method allocates a lower damper. This lower damper at the top floor enables it to have larger motions and hence results in higher levels of supplementary damping despite the higher value on the lower floors. This is especially noticeable for the linear damper, for α = 1, or the nonlinear case with α=0.5.

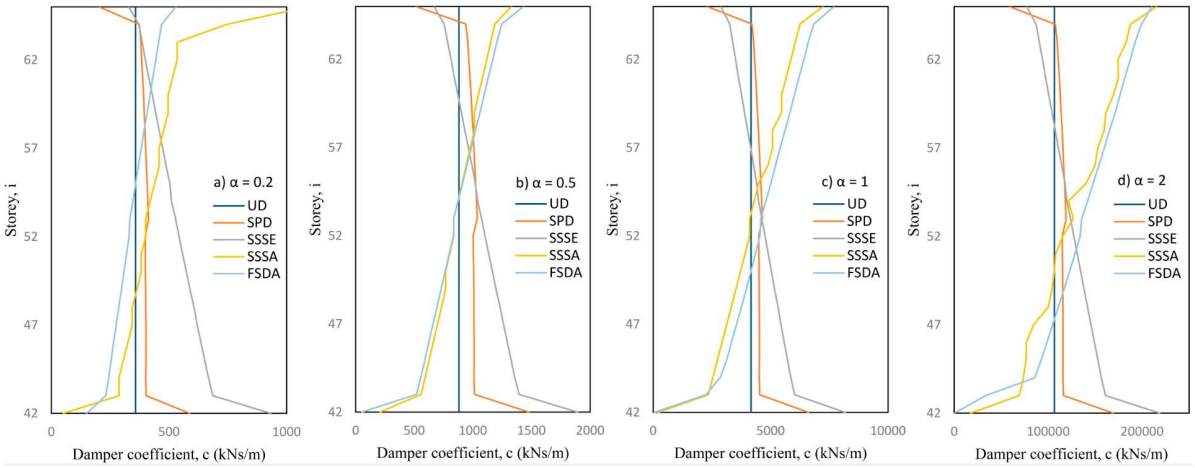

Figure 8: Optimal damper coefficient allocation along the height for each damper exponent and placement method

Table 6: Optimal damper coefficient distributions for various damper placement methods, for α = 0.2 and α = 0.5

	Damper coefficient (kNs/m) - α = 0.2					Damper coefficient (kNs/m) - α = 0.5				
Storey	**UD**	**SPD**	**SSSE**	**SSSA**	**FSDA**	**UD**	**SPD**	**SSSE**	**SSSA**	**FSDA**
65	358	214	319	1015	584	881	514	668	1328	1431
64	358	391	360	538	521	881	939	755	1188	1246
63	358	398	374	508	505	881	956	784	1153	1204
62	358	402	388	498	492	881	965	813	1118	1169
61	358	406	401	478	478	881	975	841	1083	1132
60	358	410	415	477	464	881	984	871	1048	1096
59	358	413	430	458	452	881	992	901	1013	1061
58	358	417	444	439	437	881	1001	931	1013	1022
57	358	420	458	420	424	881	1009	961	978	986
56	358	424	473	420	411	881	1016	991	943	950
55	358	427	487	401	398	881	1024	1021	908	913
54	358	430	495	382	385	881	1031	1039	873	876
53	358	433	511	382	371	881	1038	1072	838	836
52	358	418	526	363	366	881	1002	1103	838	833
51	358	419	541	363	353	881	1004	1134	803	799
50	358	419	556	344	341	881	1006	1165	768	764
49	358	420	571	325	329	881	1008	1196	768	729
48	358	420	587	325	317	881	1009	1230	733	695
47	358	421	601	306	304	881	1009	1260	698	659
46	358	421	616	287	292	881	1010	1292	663	625
45	358	421	632	287	281	881	1010	1325	628	592
44	358	420	647	268	268	881	1009	1356	593	557
43	358	422	665	249	255	881	1013	1395	558	518
42	358	615	903	50	172	881	1477	1893	208	53

Table 7: Optimal damper coefficient distributions for various damper placement methods, for α = 1 and α = 2

	Damper coefficient (kNs/m) - α = 1					Damper coefficient (kNs/m) - α = 2				
Storey	**UD**	**SPD**	**SSSE**	**SSSA**	**FSDA**	**UD**	**SPD**	**SSSE**	**SSSA**	**FSDA**
65	4167	2301	2886	7228	7703	106667	58908	77178	215431	210330
64	4167	4204	3259	6253	6834	106667	107641	87168	187499	199253
63	4167	4280	3383	6058	6606	106667	109582	90481	183099	192491
62	4167	4322	3512	5863	6417	106667	110656	93921	174452	187497
61	4167	4368	3631	5668	6209	106667	111843	97120	174773	181798
60	4167	4408	3761	5473	6015	106667	112854	100576	169413	176494
59	4167	4444	3890	5473	5828	106667	113771	104045	161518	171347
58	4167	4484	4020	5083	5614	106667	114803	107503	159593	165288
57	4167	4519	4150	5083	5414	106667	115703	110974	152771	159669
56	4167	4553	4279	4888	5214	106667	116568	114446	149711	153904
55	4167	4586	4409	4498	5012	106667	117408	117916	140388	147960
54	4167	4617	4485	4303	4807	106667	118218	119953	121567	142072
53	4167	4650	4629	4108	4582	106667	119063	123793	126704	135736
52	4167	4490	4762	4108	4554	106667	114947	127365	115345	133907
51	4167	4499	4896	3913	4357	106667	115185	130943	108010	128406
50	4167	4507	5030	3718	4162	106667	115387	134530	106390	122741

49	4167	4514	5165	3523	3963	106667	115560	138124	104122	116905
48	4167	4517	5311	3328	3760	106667	115653	142035	100077	110862
47	4167	4522	5441	3133	3555	106667	115763	145513	84431	104660
46	4167	4523	5576	2938	3343	106667	115796	149135	76900	98548
45	4167	4522	5722	2743	3138	106667	115768	153020	76303	92565
44	4167	4519	5855	2548	2868	106667	115700	156582	73725	85697
43	4167	4536	6023	2353	2248	106667	116141	161065	69281	33565
42	4167	6614	8174	208	50	106667	169333	218613	17632	50

5.2 Seismic response

The seismic performance of a building is significantly enhanced in the presence of an IDS system, in comparison with a rigid counterpart. This is demonstrated through the typical response depicted in Figure 9, where the top displacement is plotted, for illustrative purposes, for both the rigid case and that with the IDS (using a linear damper, a UD optimum distribution for the 00302T record and for three damper exponents).

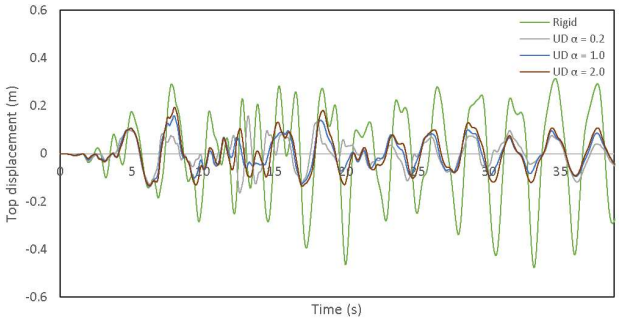

Figure 9: Displacement time history under the 00302T record for the optimised linear damper using a UD distribution

As shown in Figure 10, the top displacement is greatly reduced for all seismic records irrespective of the damper exponent or damper placement method considered. Whilst the response depends on the specific characteristics of the earthquake excitation [17], there are clear trends in terms of the benefits of IDS, as well as the performance of the different placement methods. Although all placement methods at their optimal damper coefficients appear to offer broadly similar performance, the UD, SPD, and SSSE approaches provide better performance than SSSA and FSDA. The largest reduction in top displacement, of about 73%, when compared to the fixed case, is achieved with a damper exponent of 0.2 and an FSDA distribution for the 00302T record. The smallest reduction is also for a damper exponent of 0.2 under the SSSA distribution for the 00293T record where the reduction is only about 3%. As indicated in Figure 10, the damping distribution does not make a notable difference, yet it is possible to observe how the response of the system varies depending on the seismic excitation.

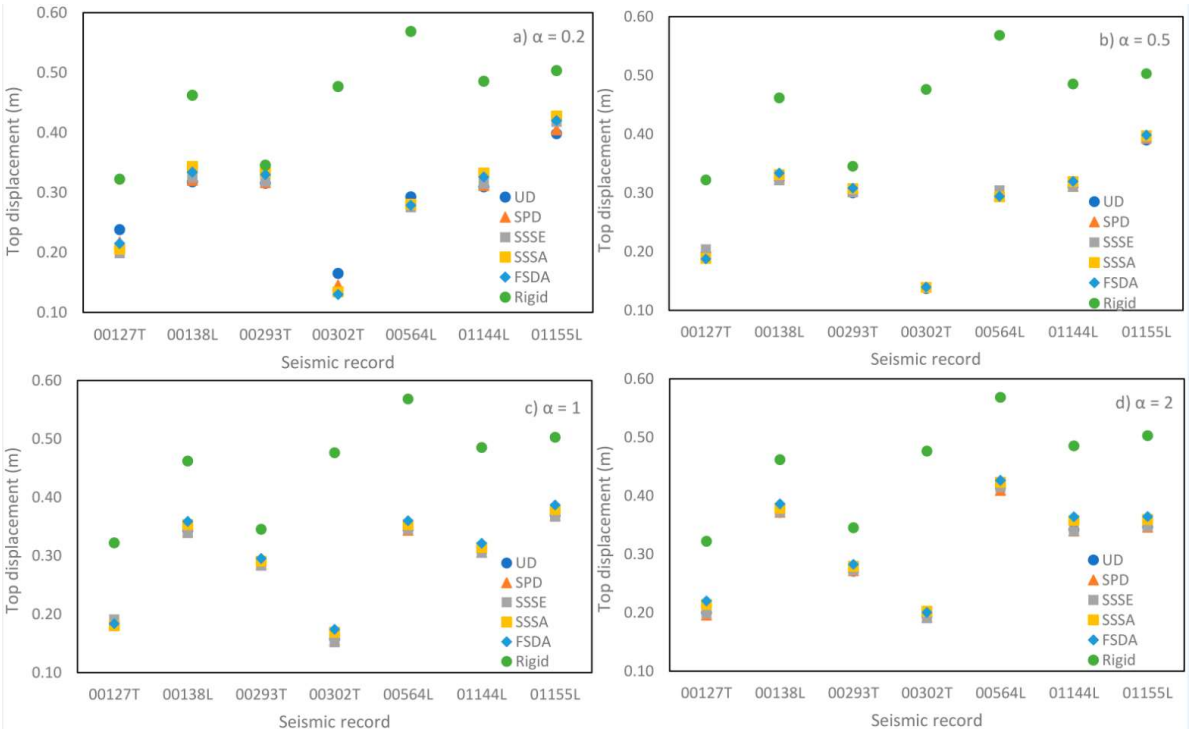

Figure 10: Maximum top displacement under selected earthquake records for each damper placement method and damper exponent, a) α = 0.2, b) α = 0.5, c) α = 1 and d) α = 2

The average top displacement reduction ratio for the seven records is depicted in Figure 11 together with the standard deviation for the seven records. Evidently, the use of IDS greatly improves the seismic response, reducing the average top displacement within 29 % to 38 %. Amongst the considered damper exponents, 0.5 offers the best performance with also the least variability between the placement methods. In contrast, α = 2 results in less reduction and more inconsistency between the results of the various placement methods.

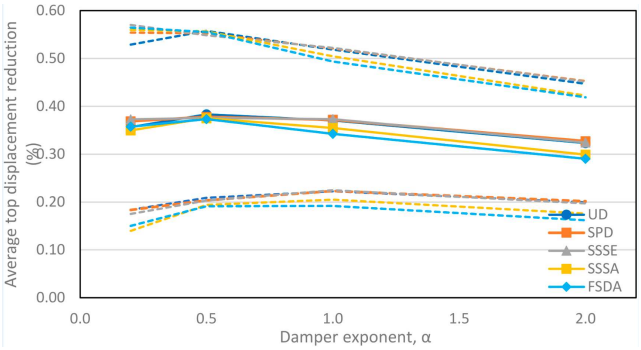

Figure 11: Average reduction ratio in top displacement vs damper exponent for the seven records and different placement methods. (sandard deviations across the seven records are included as dashed lines)

The inter-storey drifts also reduce in the presence of the IDS when compared to the rigid case (Figure 12). Despite the larger flexibility of the office floors engaged as damper mass, due to the spring allowing differential motions, the inter-storey drifts are noticeably reduced at the levels at which the IDS is implemented. Since the damper floors behave as a TMD moving opposite to the rest of the building, a large inter-storey drift can be observed at the 9 m high transition level, reaching about 1% drift. Although this might seem excessive for conventional cladding systems, it is worth noting that transition levels can be designed as MEP floors, typically provided with louvres on the façade which can be purposely designed to accommodate such drift levels. Even though all damped floors are connected by nominally pinned columns, allowing them to move independently from their contiguous members, the inter-storey drifts are considerably reduced within the damper floors when compared to those from a rigid model. Gravity columns could be designed to be fixed throughout the height, and although they would not provide any significant overall lateral stiffness, they would help smoothen the floor movements should this be an issue for a different application or at locations such as the step when the estimated drift could not be accommodated.

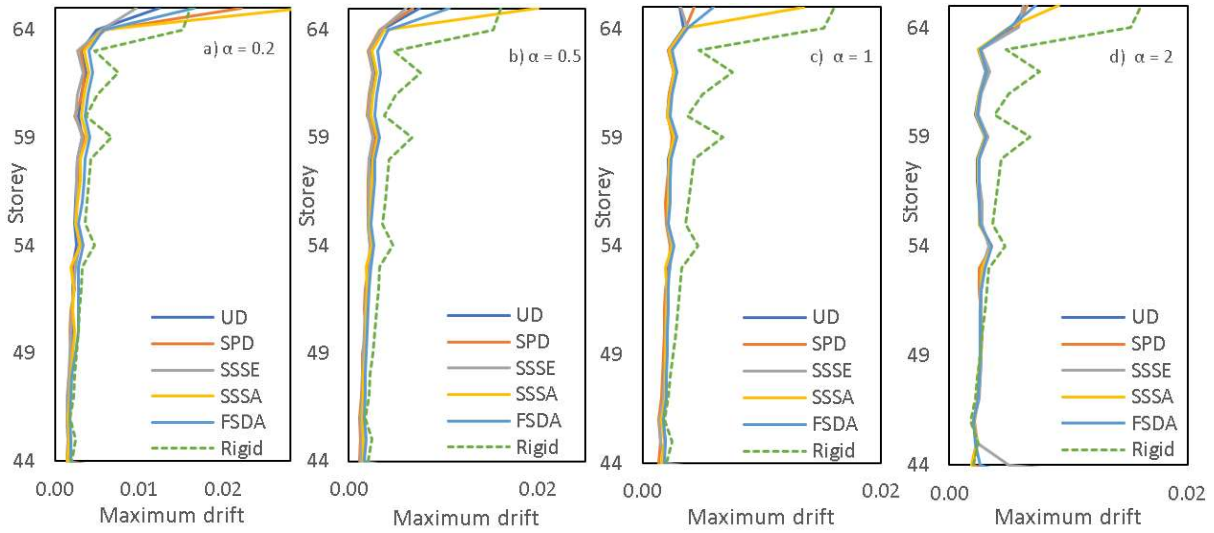

Figure 12: Maximum inter-storey drifts averaged over the seven records for each damper exponent and placement method, a) α = 0.2, b) α = 0.5, c) α = 1 and d) α = 2

The full set of results for all records is given in the Appendix, for compactness. Maximum inter-storey drifts are depicted in Figure A-1. It is shown that the extreme damper exponents considered, i.e. 0.2 and 2, exhibit a higher variability than 0.5 or 1, which behave in a smoother manner resulting in typically smaller inter-storey drifts. As also indicated in Figure 12, there is no notable variation between different damper placement methods. The SSSA and FSDA approaches have a larger variability, with the latter being the least favourable. The distributions arising from the SPD and SSSE methods typically result in the best performance over all the records. However, these two distributions have the disadvantage that they also lead to higher drifts at the transition storey. In this respect, the UD method is at the mid-point of the five methods. It also has a smaller peak at the transition yet still achieves a significant reduction in inter-storey drifts between the two subgroups.

The absolute accelerations at the office floors, averaged over the seven selected records, for all damper exponent and damper placement methods, are depicted in Figure 13 with the full set of results shown in Figure A-2. It is clear from the results that the seismically induced accelerations are drastically reduced when compared to the rigid case. As the floors are isolated from the main structure, they act in a similar way to a floor isolation system (FIS) and detach themselves almost completely from the large level of accelerations experienced by the rest of the building. As is the case with large mass TMDs, the levels just below where the IDS is implemented experience a slight increase in accelerations. Nonetheless, these accelerations are, at all instances, below those occurring at the rigid case and lower levels and are hence not considered to be governing the response.

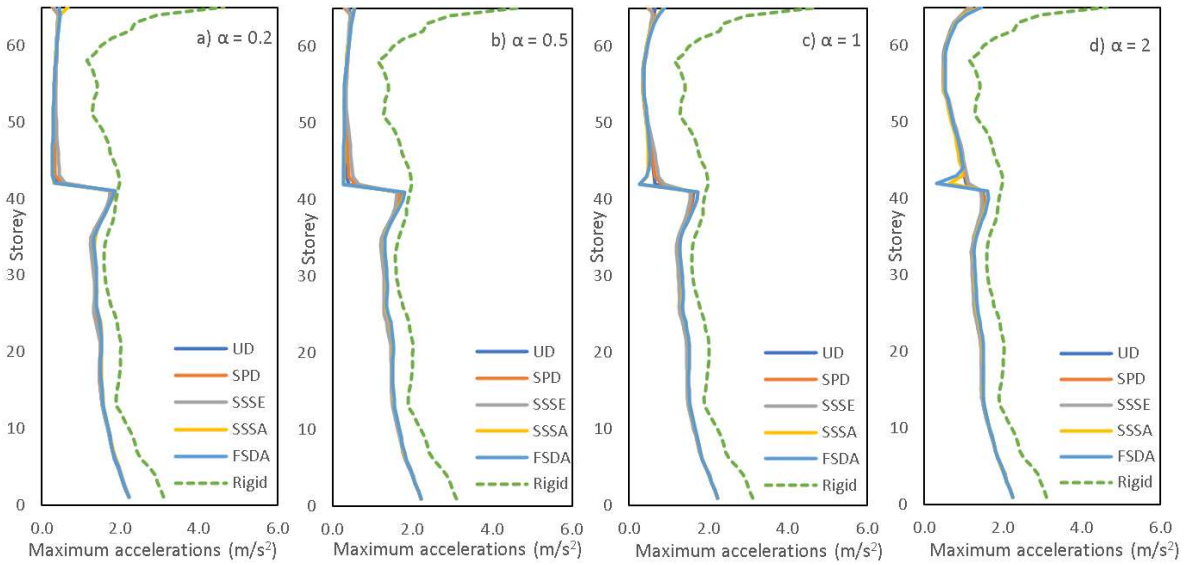

Figure 13: Maximum absolute acceleration at the office floors averaged over the seven selected records for each damper exponent and damper placement method, a) α = 0.2, b) α = 0.5, c) α = 1 and d) α = 2

From the plots in Figure 13, it is also evident that the accelerations at the damped floors increase with the damper exponent. This is particularly evident for a damper exponent value of 2. The different damper placement methods do not have any noticeable effect. The UD and the SSSA methods slightly outperform the other arrangements, yet this difference is not considered to be governing for a typical application.

Another key performance target influencing the feasibility of the system is the differential displacement between the office floors and the core. For the present study, the spring stiffness was sized to allow only 150mm differential movement for the EN1991-1-4 [59] static wind load. The maximum differential displacement throughout the whole duration averaged over the seven seismic records is plotted in Figure 14 for each damper exponent and damper placement method. The full set of results is given in Figure A-3.

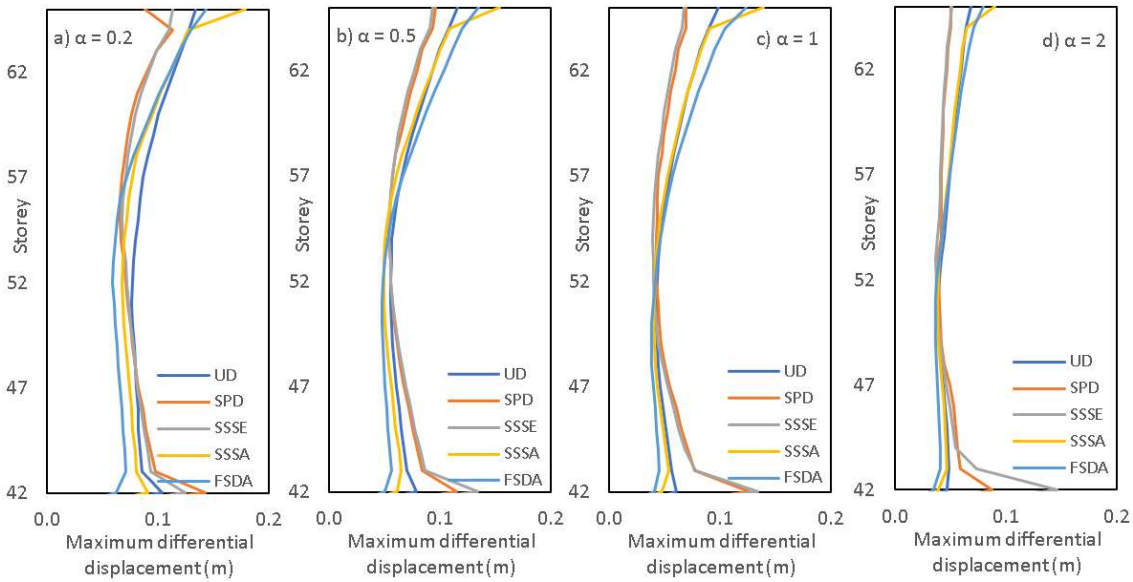

Figure 14: Average of the maximum differential displacements for the selected seismic records per storey, a) α = 0.2, b) α = 0.5, c) α = 1 and d) α = 2

The results show that the maximum differential displacements for all records are largely within those defined for serviceability wind loads, and hence show the overall feasibility of the concept and, more specifically, of the approach of defining spring stiffness based on the serviceability loads. Although this will obviously depend on the intensity of the wind and seismic actions for each application, no unexpectedly large motions have taken place due to typical seismic excitations. As with conventional FVD design, an increased stroke length and gap will have to be specified in order to avoid the risk of pounding under the Maximum Considered Earthquake excitation beyond that defined for serviceability conditions.

It is worth noting that the top and lower movable floors experience relatively larger motions than others, which matches the larger inter-storey drifts that were also previously observed in these locations. A single stiffness target was identified in the present study, yet this may be an area worthy of future research. Large variability is observed between individual seismic records for each placement method and damper exponent. This is particularly noticeable for the upper and lower bound exponents, $\alpha = 0.2$ and $\alpha = 2$, whilst a relatively smooth behaviour was obtained for $\alpha = 0.5$ and $\alpha = 1$.

As mentioned before, the FSDA placement method is intended to minimize the differential displacement between the core and the movable floors, hence it offers lower levels of motion in this case. However, this is especially noticeable for the lower floors rather than the top levels. The reason for this is that the damper placement was performed under a wind-based first-mode load pattern, and hence it is not as effective for seismic excitations. As expected from the previously plotted damper distributions, the SPD and SSSE, which are the two best-performing methods, result in larger differential displacements at the base yet higher at the top. From the five methods, and contrary to previous favourable performance indications, the UD is comparatively less effective in terms of maximum differential displacements. However, despite such discrepancies between the various placement methods, more significant and dominant differences in performance can be observed by changing the damper exponent, with the maximum differential displacements notably decreasing with the increased damper exponent. For example, the maximum differential displacements under $\alpha = 2$ are 40-45 % smaller than for $\alpha = 0.2$.

The damper forces at each storey level, averaged over the seven records for all placement methods and damper exponents, are depicted in Figure 15, while the full results are shown in Figure A-4. As expected, based on Equation (1), a significant correlation exists between damper forces and damper exponent, noting that the larger the damper exponent, the larger the forces are. It is also interesting to note that the force distribution varies with the damper exponent, with lower damper exponents resulting in a more constant distribution. In contrast, for higher values, especially for $\alpha = 2$, the distribution follows a nonlinear pattern which peaks at the higher floors.

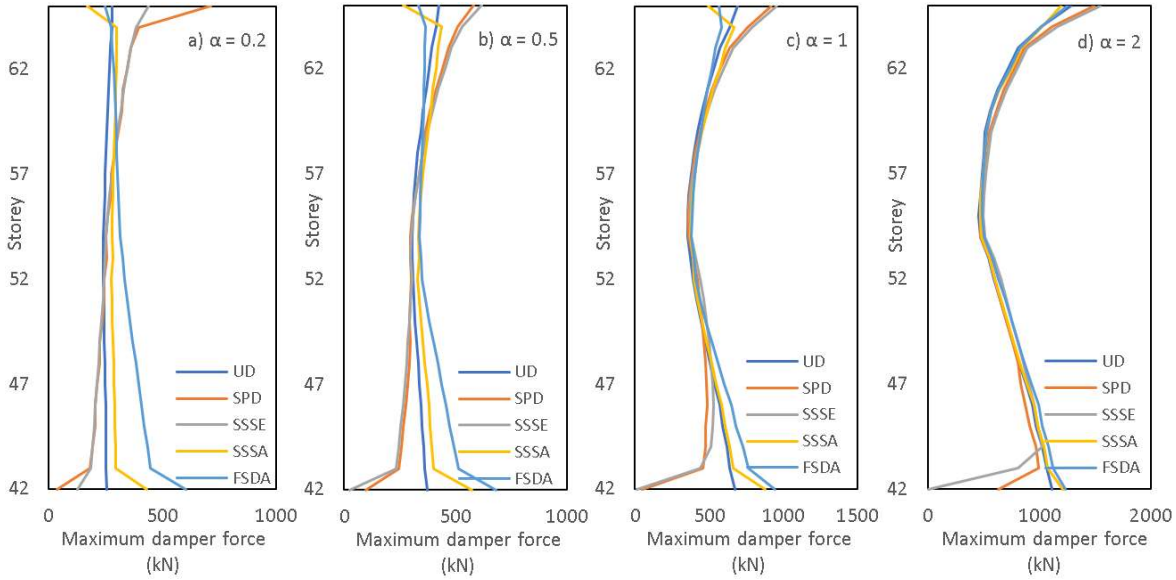

Figure 15: Maximum damper forces averaged over the seven records for each damper exponent and placement method, a) α = 0.2, b) α = 0.5, c) α = 1 and d) α = 2

Besides the local high points and varying force distribution, no damper placement method seems to clearly outperform the rest or lead to very large forces. The SSSA method results in lower forces overall and especially as the damper exponent increases. This is attributed to the formulation of this method, which relies on placing dampers at the storeys with higher velocities, and hence as the damper exponent increases the velocity term is smaller when compared to other methods. Overall, the UD offers a lower level of forces, only slightly smaller than those observed in the FSDA. The SPD and SSSE methods, on the other hand, exhibit the larger forces independently of the damper exponents.

5.3 Comparative evaluations

In the previous section, the performance of each of the indexes considered was examined for each storey in the building. To provide an overall comparative assessment of the response, table 8 compiles the key performance indicators for the various placement methods averaged over all storeys as well as for all records.

Table 8: Performance index averaged over all storeys and seismic records, for various damper placement methods and damper exponent values.

Response parameter	**α = 0.2**					**α = 0.5**				
	UD	**SPD**	**SSSE**	**SSSA**	**FSDA**	**UD**	**SPD**	**SSSE**	**SSSA**	**FSDA**
Average top displacement reduction	36%	35%	36%	37%	37%	38%	38%	37%	38%	38%
Average drift reduction throughout the whole height	22%	7%	13%	6%	19%	32%	23%	25%	28%	25%
Average acceleration reduction throughout the whole height	27%	25%	26%	26%	26%	28%	27%	26%	27%	27%
Average differential displacement (mm)	92	87	79	83	84	72	69	69	70	71
Average damper force (kN)	253	289	347	274	265	345	376	398	333	331
Response parameter	**α = 1.0**					**α = 2.0**				
	UD	**SPD**	**SSSE**	**SSSA**	**FSDA**	**UD**	**SPD**	**SSSE**	**SSSA**	**FSDA**
Average top displacement reduction	37%	35%	34%	37%	37%	32%	30%	29%	33%	32%
Average drift reduction throughout the whole height	36%	28%	31%	25%	23%	30%	28%	25%	22%	9%
Average acceleration reduction throughout the whole height	25%	24%	24%	25%	25%	20%	19%	18%	20%	20%
Average differential displacement (mm)	58	57	58	57	55	50	49	48	48	50
Average damper force (kN)	496	515	533	470	490	750	761	782	744	747

The reported values illustrate the feasibility and favourable performance of the IDS system under a wide range of key parameters. From the results in Table 8, the average reduction in top displacement ranges from 29 to 38%. Despite the local peak at the transition storey, the overall drifts are also reduced by 6 to 36%. The average reduction in absolute accelerations for the whole building is in the range of 18 to 28%. On the other hand, the average differential displacements under seismic loading are also well below the predefined serviceability wind case, ranging from 92 mm for $\alpha = 0.2$ and a UD method, to 48 mm for $\alpha = 0.2$ and SSSE or SSSA distributions. Finally, although the average damper forces triple from $\alpha = 0.2$ to $\alpha = 2$, their magnitude is observed to be relatively easy to control within conventional design if properly accounted for.

Based on the reported results, the following observations and recommendations can be highlighted in relation to damper placement method and damper exponent selection.

- For cases where wind is the governing parameter, using a lower damper exponent, $\alpha = 0.2$ or $\alpha = 0.5$, and a UD distribution can maximise the level of damping to meet the required target, reducing differential displacements with low damper forces.
- Damper exponents of 0.5 and 1 offer the best seismic performance when all parameters are taken into consideration. The value of 0.5 provides a slightly better performance and results in smaller damper forces yet slightly larger differential displacements. Where differential displacements need to be tightly controlled, a damper exponent of $\alpha = 2$ offers the best results.
- The UD, SPD, and SSSE methods offer the most favourable overall performance. However, it should be noted that UD benefits from the regular and uniform building configuration adopted in this study, which may differ in other cases. On the other hand, SPD and SSSE methods provide the best performance under seismic excitations and can also be adapted to any building configuration.
- Although the FSDA or SSSA methods are not the best-performing in terms of overall response, it should be noted that they could be of interest where it would be desirable to specifically reduce the differential displacements or damper forces, respectively.

With the inclusion of the IDS, it was possible to provide up to 6.2% additional equivalent damping. Besides the improvement in seismic performance, this additional damping led to a significant reduction in passive wind and dynamic loads. This level of damping can suppress any wind excitation and control wind-induced accelerations. With this increase in damping, it was possible to mitigate wind-induced accelerations from the initial yearly peak of 17.7 mg down to 6 mg, which is well within the typical comfort limits for an office or residential building.

6. Conclusions

This paper has examined the performance of the novel Integrated Damping System (IDS) approach, with particular focus on the characteristics and distribution of the constituent Fluid Viscous Dampers (FVD). The recently introduced IDS arrangement offers large levels of damping by enabling two parts of a building to move independently yet controls this differential motion through springs and dampers in parallel. In order to provide a practical perspective and detailed insights into the behaviour, the assessments presented in this paper were illustrated through the dynamic response of a typical 300m tall building incorporating the IDS alongside a conventional internal core arrangement. The key parameters related to the FVDs performance, as well as their alternative placement methods within a structure, were firstly discussed. This was followed by detailed evaluations with respect to the optimal damper parameters and arrangement.

Besides examining the overall system performance, five different damper placement methods were investigated, namely uniform distribution (UD), stiffness proportional distribution (SPD), storey shear strain energy (SSSE), simple sequential search algorithm (SSSA), and the full analysis design/redesign algorithm (FSDA). The five methods were applied to both linear and nonlinear damper exponents (α), with values of 0.2, 0.5, 1, and 2. System's performance and behaviour was analysed under typical wind conditions as well as seven selected natural seismic excitations.

The results of the investigation provided detailed insights into the behavioural benefits of the IDS approach as well as the key parameters influencing its optimal application in tall buildings. It was shown that an additional 6.2% of equivalent damping could be generated, enabling the building to control wind-induced accelerations within user-comfort levels, and reducing both static and dynamic wind loads. Moreover, the seismic performance of the building clearly outperformed that of a conventional rigid counterpart. It was shown that the top displacement of the structure under seismic loading was reduced by an average of 29-38% with respect to the

rigid case. The average inter-storey drifts over the whole building were also reduced by 6-36%. Furthermore, the seismically induced accelerations within the structure were reduced by a range of 18% to 28%. The average differential displacements also remained within serviceability values, ranging from 48 mm to 92 mm. Moreover, the average damper force remained within practical limits, ranging between 253 kN to 782 kN.

Unless a specific performance parameter is aimed for, it was shown that the intermediate damper exponent values of 0.5 and 1.0, resulted in the most favourable overall response and are hence recommended for design applications. The damper exponent, α, was shown to be a key parameter influencing the response. For applications in which the design involves targeting a specific performance, the results of this investigation suggest the following optimal parameters: (i) additional damping, with exponent $\alpha = 0.2$ and UD arrangement; (ii) reduced top displacement, with damper exponent $\alpha = 0.5$ and UD placement method; (iii) reduced inter-storey drifts, with $\alpha = 1$ and UD distribution; (iv) reduced accelerations, with $\alpha = 0.5$ and UD distribution; (v) reduced differential displacements, with $\alpha = 2$ and FSDA or SSSA placement; (iv) reduced damper forces, with $\alpha = 0.2$ and FSDA or SSSA distribution.

Importantly, the results of this study reveal that due to the underlying nature of the IDS approach, which acts as a large-mass damper, its overall performance is not highly sensitive to the damper placement method and does not necessitate the use of an advanced distribution to mobilise its full potential. Accordingly, although specific placement methods can be adopted to refine particular performance aspects where necessary, simple and practical damper arrangements, such as the uniform or stiffness proportional distributions, can be consistently employed in conjunction with the IDS to provide a most favourable and highly effective solution.

References

1. Nielsen E. J., M. Lai, T. T. Soong, J. M. Kelly, (1996) Viscoelastic damper overview for seismic and wind applications, in Smart Structures and Materials, Society of Photo-Optical Instrumentation Engineers, San Diego, CA, United states 1996: Passive Damping and Isolation. Feb 26-27 96 138 10.1117/12.239081.
2. Constantinou, M. C., & Symans, M. D. (1993). Seismic response of structures with supplemental damping. The Structural Design of Tall Buildings, 2(2), 77–92. doi:10.1002/tal.4320020202
3. Taylor, D. (2003) Mega Brace Seismic Dampers for the Torre Mayor Project at Mexico City. Taylor Devices Technical Report. www.taylordevices.com [10 July 2016]
4. Constantinou M. C., P. Tsopelas, W. Hammel, A. N. Sigaher, J. Struct. Eng. 2001, 127(2), 105. https://doi.org/10.1061/(asce)0733-9445(2001)127:2(105)
5. McNamara, R. J, & Taylor, D. P. Struct. Des.Tall Spec. Build. 2003, 12(2), 145. https://doi.org/10.1002/tal.218
6. Trabucco, Dario, et al, (2018) Damping technologies for Tall Buildings. Elsevier Science & Technology, CTBUH
7. Smith, R & Willford, M. (2007) The damped Outrigger concept for tall buildings. Struct. Design Tall Spec. buildings, 16, pp 501-517, doi:10.100/tal.413
8. Ormondroyd, J. & Den Hartog, J. P. The theory of dynamic vibration absorber. Trans. ASME 1928. APM-50-7, 9-22.
9. Den Hartog, J. P. Mechanical vibrations. 34th ed, McGraw-Hill, New York 1956.
10. Gutierrez Soto, M. & Adeli, H. Tuned Mass Dampers. Arch. Comput Methods Eng 2013. 20: 419-431. doi:10.1007/s11831-013-9091-7
11. Kwok, K. C. S. & Samali, B. Performance of tuned mass dampers under wind loads. Engineering Structures 1995. Elsevier Science LTd. Great Britain. Vol. 17, No. 9 pp. 655-667. doi:10.1016/0141-0296(95)00035-6.
12. Gutierrez Soto, M. & Adeli, H. Recent advances in control algorithms for smart structures and machines. Expert Systems 2017. Vol. 34. No. 2:e12205. doi:10.1111/exsy.12205
13. Lee, C., Chen, Y., Chung, L & Wang, Y. Optimal design theories and applications of tuned mass dampers. *Engineering Structures* **2006** Elsevier Science LTd. Great Britain. Vol 28. No. 1, pp 43-53. doi:10.1016/j.engstruct.2005.06.023.
14. Aly, A.M. Control of wind-induced motion in high-rise buildings with hybrid TM/MR dampers. *Wind and Structures* **2015**, 21(5), pp 565-595. doi: 10.12989/was.2015.21.5.565.
15. Feng, M. & Mita, A. Vibration Control of Tall Buildings Using Mega SubConfiguration. *Journal of Engineering Mechanics*, ASCE **1995**; 121;1082-1088. doi: 10.1061/(ASCE)0733-9399(1995) 121:10(1082)
16. El-Khoury, O. & Adeli, H. Recent Advances on Vibration Control of Structures Under Dynamic Loading. Arch Comput Methods Eng 2013. 20, pp 353-360. doi: 10.1007/s11831-013-9088-2
17. Martinez-Paneda, M. and Elghazouli, A. Y. "An integrated Damping System for Tall Buildings", The Structural Design of Tall and Special Buildings, 29(7), (2020), e1724.
18. Soong, T. T. & Dargush, G.F. Passive energy dissipation systems in structural engineering. John Wiley & Sons Chichester, 1997 ISBN 0-471-96821-.8
19. Hwang, J.; Lin,. W. & Wu, N. Comparison of distribution methods for viscous damping coefficients to buildings. Structure and Infrastructure Engineering (2013), 9-1, pp 28-41, doi: 10.1080/15732479.2010.513713
20. Adachi, F., Fujita, K., Tsuji, M. & Takewaki, I. Importance of interstory velocity on optimal along-height allocation of viscous oil dampers in super high-rise buildings. Engineering Structures (2013), Vol 56, pp 489-500. doi:10.1016/j.engstruct.2013.05.036.
21. De Silva C.W., An algorithm for the optimal design of passive vibration controllers for flexible systems, *Journal of Sound and Vibration*, Volume 75, Issue 4, 1981, Pages 495-502, ISSN 0022-460X, doi:10.1016/0022-460X(81)90437-5.
22. Gürgöze M. & P.C. Müller. Optimal positioning of dampers in multi-body systems. Journal of Sound and Vibration, Volume 158, Issue 3, 1992, Pages 517-530, ISSN 0022-460X, doi:10.1016/0022-460X(92)90422-T.
23. Landi, L; Conti, F. & Diotallevi, P.P. Effectiveness of different distributions of viscous damping coefficients for the seismic retrofit of regular and irregular RC frames. Engineering Structures, Vol 100, 2015, pp 79-93, doi:10.1016/j.engstruct.2015.05.031.
24. Saitua, F.; Lopez-Garcia, D.; Taflanidis, A. A.; Optimization of height-wise damper distributions considering practical design issues. Engineering Structures (2018) Volume 173, Pages 768-786, ISSN 0141-0296, doi:10.1016/j.engstruct.2018.04.008.

25. Lavan O, Levy R. Optimal design of supplemental viscous dampers for irregular shear-frames in the presence of yielding. Earthq Eng Struct Dyn 2005;34(8):889–907.
26. Cimellaro GP, Lavan O, Reinhorn AM. Design of passive systems for control of inelastic structures. Earth Eng Struct Dyn 2009;38(6):783–804.
27. Lavan, O & Levy, R. Optimal peripheral drift control of 3d irregular framed structures using supplemental viscous dampers. J Earth Eng, 2006. 10(6), pp 903-23
28. Lavan O. Optimal design of viscous dampers and their supporting members for the seismic retrofitting of 3D irregular frame structures. J Struct Eng 2015; 141(11):04015026.
29. Impollonia, N, Palmeri, A. Seismic performance of buildings retrofitted with nonlinear viscous dampers and adjacent reaction towers. Earthquake Engng Struct Dyn. 2018; 47 1329– 1351. Doi:10.1002/eqe.3020
30. Whittle JK, Williams MS, Karavasilis TL, Blakeborough A. A comparison of viscous damper placement methods for improving seismic building design. J Earth Eng 2012; 16(4): 540-60
31. Lin, T.K.; Hwang, J.S. & Chen, K.H. Optimal Distribution of Damping Coefficients for Viscous Dampers in Buildings. International Journal of Structural Stability and Dynamics, 2017. 17-4 1750054, doi: 10.1142/S0219455417500547
32. Del Gobbo, G.; Williams, M.S. & Blakeborough, A. Comparing fluid viscous damper placement methods considering total-building seismic performance. Earthquake Engineering and Structural Dynamics (2018). 1-23. Doi: 10.1002/eqe.3117
33. Domenico, D.; Ricciardi, G. &Takewaki, I. Design strategies of viscos dampers for seismic protection of building structures: A Review. Soil Dynamics and Earthquake Engineering, 2019. 118, 144-165. Doi: 10.1016/j.soildyn.2018.12.024
34. Hwang, J., Huang, Y., Yi, S & Ho, S. Design Formulations for Supplemental Viscous Dampers to Building Structures (2008) Journal of Structural Engineering V134-1, pp 22-31 doi:10.1061/(ASCE)0733-9445(2008)134:1(22)
35. Gluck N, Reinhorn AM, Gluck J, Levy R. Design of supplemental dampers for control of structures. J Struct Eng 1996;122(12):1394–9.
36. Takewaki, I. (1997), Optimal damper placement for minimum transfer functions. Earthquake Engng. Struct. Dyn., 26: 1113-1124. doi:10.1002/(SICI)1096-9845(199711)26:11<1113::AID-EQE696>3.0.CO;2-X
37. Levy R, Lavan O. Fully stressed design of passive controllers in framed structures for seismic loadings. Struct Multidiscip Optim 2006;32:485–98.
38. Singh MP, Moreschi LM. Optimal placement of dampers for passive response control. Earthq Eng Struct Dyn 2002;31:955–76.
39. Fujita, K.; Yamamoto, K. & Takewaki, I. An evolutionary algorithm for optimal damper placement to minimize interstorey-drift transfer function in shear building. Earthquakes and Structures (2010). Vol 1-3, pp 289-306
40. Parcianello, E.; Chisari, C. & Amadio, C. Optimal design of nonlinear viscous dampers for frame structures. Soil Dynamics and Earthquake Engineering (2017). 100, pp 257-260, doi: 10.1016/j.soildyn.2017.06.006
41. Doflot P. and Taylor D. (2008). Experience and practical considerations in the design of viscous dampers, *Proceedings of 3rd international conference on footbridge*, Porto, Portugal.
42. Lin, W-H., and Chopra, A. K. (2002). Earthquake response of elastic SDF systems with nonlinear fluid viscous dampers, *Earthquake Engineering & Structural Dynamics,* 31: 1623-1642.
43. Li, A. Vibration control for building structures: Theory and Applications. Springer, 2020. doi.org/10.1007/978-3-030-40790-2_5
44. Symans, M.D., Constantinou, M.C. (1998). Passive fluid viscous damping systems for seismic energy dissipation, *ISET Journal of Earthquake Technology*, 35(4): 185□206.
45. Bahnasy, A & Lavan, O. Linear or nonlinear fluid viscous dampers? A seismic point of view. Structures Congress 2013.
46. Lee, D. & Taylor, P. Viscous damper development and future trends. Struct. Design Tall Build, 2001. 10, 311-320. Doi: 10.1002/tal.188
47. Wang, S. Enhancing seismic performance of Tall Buildings by Optimal Design of Supplemental Energy-Dissipation Devices. PhD Thesis, 2017, U.C. Berkeley
48. Di Sarno, L., & Elnashai, A. S. (2005). Innovative strategies for seismic retrofitting of steel and composite structures. PROGRESS IN STRUCTURAL ENGINEERING AND MATERIALS, 7(3), 115-135. doi:10.1002/pse.195
49. Gidaris, I. & Taflanidis, A. Performance assessment and optimization of fluid viscous dampers through life-cycle cost criteria and comparison to alternative design approaches. Bulletin of Earthquake Engineering, 2015, 13, 1003-1028. doi. 10.1007/s10518-014-9646-5
50. Zhang, R. & Soong, T.T. Seismic Design of Viscoelastic Dampers for Structural Applications. Journal of Structural Engineering, 1992. 1375-1392, V 118-5. doi:10.1061/(ASCE)0733-9445(1992)118:5(1375).

51. Lopez Garcia D. A simple method for the design of optimal damper configurations in MDOF structures. Earthquake Spectra 2001; 17(3):387–398.
52. Lopez Garcia, D. & Soong, T.T. Efficiency of a simple approach to damper allocation in MDOF structures. Journal of Structural Control, 2002; 9: 19-30, doi:10.1002/stc.3
53. Singh MP, Verma NP, Moreschi LM. Seismic analysis and design with Maxwell dampers. J Eng Mech 2003; 129:273–82
54. Chen YT, Chai YH. Effects of brace stiffness on performance of structures with supplemental Maxwell model-based brace-damper systems. Earth Eng Struct Dyn 2011;40(1):75–92.
55. Seleemah A, Constantinou MC. Investigation of seismic response of buildings with linear and nonlinear fluid viscous dampers. Report No. NCEER 97 0004, Buffalo, N.Y.; 1997.
56. CSI (Computer and Structures Inc.). ETABS v18 Integrated Finite Element Analysis and Design of Structures, 2020. CSI, Berkeley.
57. CEN. Eurocode 3: Design of steel structures. Part 1-1: General rules and rules for buildings. 2005, BS EN 1993-1-1:2005
58. BSI, EN 10365:2017 Hot rolled steel channels, I and H sections- Dimensions and masses 2017, British Standards Institute, BSI Standards Limited.
59. CEN. Eurocode 1: Action on Structures. Part 4: General actions – Wind actions. 2010, BS EN 1991-1-4:2005+A1:2010
60. NRCC. National Building Code of Canada 2010, Associate Committee on the National Building Code, National Research Council of Canada, Ottawa, Ont.
61. Smith, R., Merello, R., & Willford, M. Intrinsic and supplementary damping in tall buildings. Proceedings of the Institution of Civil Engineers, Structures and Buildings, 2010. V 163-2 pp 111-118. Doi: 10.1680/stbu.2010.163.2.111
62. Taranath, B.S. Structural Analysis and Design of Tall Buildings. Steel and Composite construction. CRC Press, Boca Raton 2012.
63. International Organisation for Standardization. ISO 10137:2007 Bases for design of structures – Serviceability of buildings and walkways against vibrations, 2007. Geneva, ISO.
64. CSI (Computer and Structures Inc.). SAP2000 v21.0.0 Integrated Finite Element Analysis and Design of Structures, 2020. CSI, Berkeley.
65. Chopra, A.K. Dynamics of Structures. Theory and Applications to Earthquake Engineering, 4th ed., Prentice Hall 2012, Upper Saddle River, N.J.
66. CEN. Eurocode 8: Design of structures for earthquake resistance. Part 1: General rules, seismic actions and rules for buildings. 2004, BS EN 1998-1-4:2004.
67. Beyer, K., and Bommer, J. J. (2007). "Selection and scaling of real accelerograms for bidirectional loading: a review of current practice and code provisions." Journal of Earthquake Engineering, 11(S1), 13-45.
68. PEER. NGA database (where NGA stands for “Next Generation of Attenuation”) with records orientated in fault-normal and fault-parallel orientation, PPER strong-motion database 2005. (http://peer.berkeley.edu/nga/index.html), Pacific Earthquake Engineering Research Centre, Berkeley.
69. Losanno, D., Spizzuoco, M. & Serino, G. Design and Retrofit of Multistory Frames with Elastic-Deformable Viscous Damping Braces. Journal of Earthquake Engineering 2017. Vol 23 (9). Doi: 10.1080/13632469.2017.1387193
70. Lodoño Monsalve, J. M., Wagg, D. J. & Neild S. A. Supporting brace sizing in structures with added linear viscous dampers: A filter design solution. Earthquake Engineering & Structural Dynamics 2014. Vol 43 (13): 1999-2013. Doi: 10.1002/eqe.2433
71. Takewaki, I. Critical excitation methods for important structures. Eurodyn 2008. 7th European conference on Structural Dynamics, July 2008
72. Singh MP, Moreschi LM. Optimal seismic response control with dampers. Earthq Eng Struct Dyn 2001;30(4):553–72.

Appendix

Detailed assessment at each storey level of the building for key response indicators (maximum drift, maximum absolute acceleration, maximum differential displacement, damper forces) for each of the seven selected seismic records, for different damper placement methods (UD, SPD, SSSE, SSSA, FSDA), and for various damper exponent values (0.2, 0.5, 1, 2).

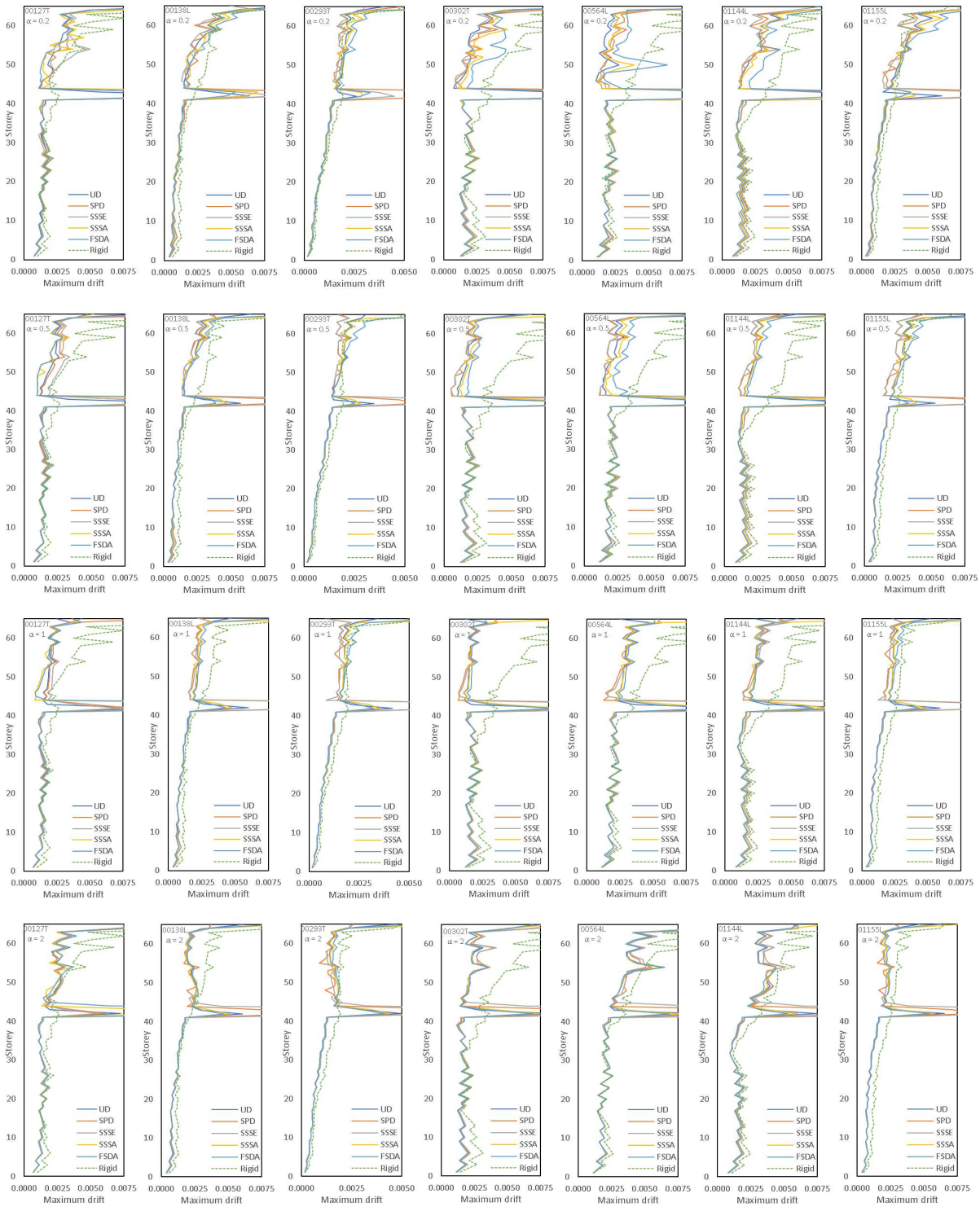

Figure A-1: Maximum inter-storey drifts for the seven records for each damper exponent and placement method.

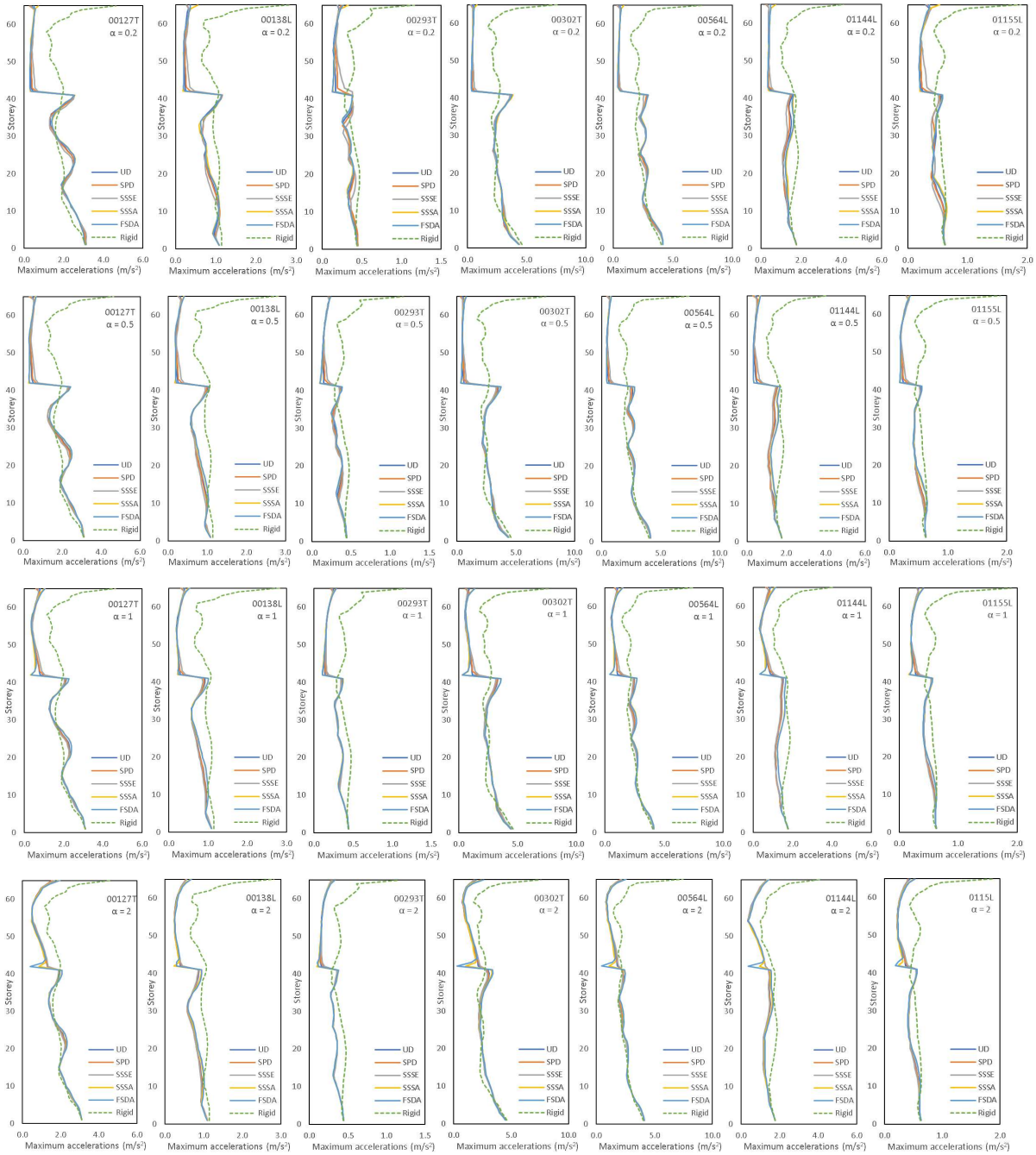

Figure A-2: Maximum absolute acceleration at the office floors for the seven records for each damper exponent and placement method.

Figure A-3: Maximum differential displacement per storey between core and movable office floors for the seven records for each damper exponent and placement method.

Figure A-4: Damper forces per storey for the seven selected seismic records for the seven records for each damper exponent and placement method.